HHS Public Access

Author manuscript

Neuroimage. Author manuscript; available in PMC 2022 November 01.

Published in final edited form as:

Neuroimage. 2021 November ; 243: 118530. doi:10.1016/j.neuroimage.2021.118530.

Connectome 2.0: Developing the next-generation ultra-high gradient strength human MRI scanner for bridging studies of the micro-, meso- and macro-connectome

Susie Y. Huang[a,*], **Thomas Witzel**[b], **Boris Keil**[c], **Alina Scholz**[c], **Mathias Davids**[a], **Peter Dietz**[d], **Elmar Rummert**[d], **Rebecca Ramb**[d], **John E. Kirsch**[a], **Anastasia Yendiki**[a], **Qiuyun Fan**[a], **Qiyuan Tian**[a], **Gabriel Ramos-Llordén**[a], **Hong-Hsi Lee**[a], **Aapo Nummenmaa**[a], **Berkin Bilgic**[a], **Kawin Setsompop**[e], **Fuyixue Wang**[a], **Alexandru V. Avram**[f], **Michal Komlosh**[f], **Dan Benjamini**[f], **Kulam Najmudeen Magdoom**[f], **Sudhir Pathak**[g], **Walter Schneider**[g], **Dmitry S. Novikov**[h,i], **Els Fieremans**[h,i], **Slimane Tounekti**[a], **Choukri Mekkaoui**[a], **Jean Augustinack**[a], **Daniel Berger**[j], **Alexander Shapson-Coe**[j], **Jeff Lichtman**[j], **Peter J. Basser**[f], **Lawrence L. Wald**[a], **Bruce R. Rosen**[a]

[a] Athinoula A. Martinos Center for Biomedical Imaging, Department of Radiology, Massachusetts General Hospital, Harvard Medical School, Boston, MA, USA

[*] Corresponding author. Susie.Huang@MGH.HARVARD.EDU (S.Y. Huang).

Credit authorship contribution statement

Susie Y. Huang: Conceptualization, Methodology, Validation, Formal analysis, Investigation, Resources, Writing – original draft, Writing – review & editing, Visualization, Project administration, Funding acquisition. **Thomas Witzel:** Conceptualization, Methodology, Software, Investigation, Writing – review & editing. **Boris Keil:** Methodology, Formal analysis, Investigation, Resources, Writing – original draft, Writing – review & editing, Visualization. **Alina Scholz:** Methodology, Formal analysis, Investigation, Resources, Writing – original draft, Writing – review & editing, Visualization. **Mathias Davids:** Methodology, Formal analysis, Investigation, Resources, Writing – original draft, Writing – review & editing, Visualization. **Peter Dietz:** Methodology, Formal analysis, Writing – review & editing. **Elmar Rummert:** Methodology, Resources, Writing – review & editing, Project administration. **Rebecca Ramb:** Methodology, Resources, Supervision, Project administration, Funding acquisition. **John E. Kirsch:** Methodology, Formal analysis, Investigation, Writing – review & editing. **Anastasia Yendiki:** Conceptualization, Methodology, Software, Validation, Investigation, Resources, Writing – original draft, Visualization. **Qiuyun Fan:** Methodology, Software, Validation, Formal analysis, Investigation, Visualization. **Qiyuan Tian:** Methodology, Software, Validation, Formal analysis, Investigation, Data curation, Visualization. **Gabriel Ramos-Llordén:** Methodology, Validation, Formal analysis, Investigation, Writing – original draft, Visualization. **Hong-Hsi Lee:** Methodology, Software, Validation, Formal analysis, Investigation, Writing – original draft, Writing – review & editing, Visualization. **Aapo Nummenmaa:** Methodology, Software, Validation, Formal analysis, Investigation. **Berkin Bilgic:** Methodology, Software, Validation, Formal analysis, Investigation, Funding acquisition. **Kawin Setsompop:** Methodology, Validation, Formal analysis, Investigation, Writing – original draft, Funding acquisition. **Fuyixue Wang:** Methodology, Software, Validation, Formal analysis, Investigation, Writing – original draft, Visualization. **Alexandru V. Avram:** Methodology, Software, Formal analysis, Investigation, Writing – original draft, Visualization. **Michal Komlosh:** Methodology, Software, Formal analysis, Investigation. **Dan Benjamini:** Methodology, Software, Formal analysis, Investigation. **Kulam Najmudeen Magdoom:** Methodology, Software, Formal analysis, Investigation, Writing – original draft, Visualization. **Sudhir Pathak:** Methodology, Software, Formal analysis, Investigation, Writing – original draft, Visualization. **Walter Schneider:** Conceptualization, Methodology, Validation, Resources, Writing – original draft, Visualization, Supervision. **Dmitry S. Novikov:** Conceptualization, Methodology, Validation, Formal analysis, Investigation, Resources, Writing – original draft, Writing – review & editing, Supervision, Funding acquisition. **Els Fieremans:** Conceptualization, Methodology, Validation, Formal analysis, Investigation, Resources, Writing – original draft, Writing – review & editing, Supervision, Funding acquisition. **Slimane Tounekti:** Investigation, Visualization. **Choukri Mekkaoui:** Investigation, Writing – original draft, Visualization, Funding acquisition. **Jean Augustinack:** Validation, Investigation, Resources. **Daniel Berger:** Methodology, Investigation, Resources, Data curation. **Alexander Shapson-Coe:** Methodology, Software, Resources, Data curation. **Jeff Lichtman:** Conceptualization, Methodology, Investigation, Resources, Writing – original draft, Supervision, Funding acquisition. **Peter J. Basser:** Conceptualization, Methodology, Investigation, Resources, Writing – original draft, Supervision, Project administration, Funding acquisition. **Lawrence L. Wald:** Conceptualization, Methodology, Investigation, Resources, Writing – original draft, Supervision, Project administration, Funding acquisition. **Bruce R. Rosen:** Conceptualization, Resources, Writing – original draft, Writing – review & editing, Supervision, Project administration, Funding acquisition.

[b] Q bio Inc., San Carlos, CA, USA

[c] Institute of Medical Physics and Radiation Protection (IMPS), TH-Mittelhessen University of Applied Sciences (THM), Giessen, Germany

[d] Siemens Healthineers, Erlangen, Germany

[e] Radiological Sciences Laboratory, Department of Radiology, Stanford University, Stanford, CA, USA

[f] Eunice Kennedy Shriver National Institute of Child Health and Human Development, National Institutes of Health, Bethesda, MD, USA

[g] Learning Research and Development Center, University of Pittsburgh, Pittsburgh, PA, USA

[h] Center for Biomedical Imaging, Department of Radiology, New York University School of Medicine, New York, NY, USA

[i] Center for Advanced Imaging Innovation and Research (CAI2R), New York University School of Medicine, New York, NY, USA

[j] Department of Molecular and Cell Biology and Center for Brain Science, Harvard University, Cambridge, MA, USA

Abstract

The first phase of the Human Connectome Project pioneered advances in MRI technology for mapping the macroscopic structural connections of the living human brain through the engineering of a whole-body human MRI scanner equipped with maximum gradient strength of 300 mT/m, the highest ever achieved for human imaging. While this instrument has made important contributions to the understanding of macroscale connectional topology, it has also demonstrated the potential of dedicated high-gradient performance scanners to provide unparalleled *in vivo* assessment of neural tissue microstructure. Building on the initial groundwork laid by the original Connectome scanner, we have now embarked on an international, multi-site effort to build the next-generation human 3T Connectome scanner (Connectome 2.0) optimized for the study of neural tissue microstructure and connectional anatomy across multiple length scales. In order to maximize the resolution of this *in vivo* microscope for studies of the living human brain, we will push the diffusion resolution limit to unprecedented levels by (1) nearly doubling the current maximum gradient strength from 300 mT/m to 500 mT/m and tripling the maximum slew rate from 200 T/m/s to 600 T/m/s through the design of a one-of-a-kind head gradient coil optimized to minimize peripheral nerve stimulation; (2) developing high-sensitivity multi-channel radiofrequency receive coils for *in vivo* and *ex vivo* human brain imaging; (3) incorporating dynamic field monitoring to minimize image distortions and artifacts; (4) developing new pulse sequences to integrate the strongest diffusion encoding and highest spatial resolution ever achieved in the living human brain; and (5) calibrating the measurements obtained from this next-generation instrument through systematic validation of diffusion microstructural metrics in high-fidelity phantoms and *ex vivo* brain tissue at progressively finer scales with accompanying diffusion simulations in histology-based micro-geometries. We envision creating the ultimate diffusion MRI instrument capable of capturing the complex multi-scale organization of the living human brain –from the microscopic scale needed to probe cellular geometry, heterogeneity and plasticity, to the mesoscopic scale for quantifying

the distinctions in cortical structure and connectivity that define cyto- and myeloarchitectonic boundaries, to improvements in estimates of macroscopic connectivity.

Keywords

Connectome; Diffusion MRI; Head gradient; Peripheral nerve stimulation; Multi-scale modeling; Tissue microstructure; Axon diameter; Gray matter; Validation

1. Introduction

Mapping structural connectivity in the living human brain is essential for understanding and predicting the functional signals underlying human thought and behavior. A major challenge in studying the structural basis of brain function is the vast range of spatial scales spanned by brain networks, from synaptic circuits among individual neurons all the way to whole-brain systems (Lichtman and Denk, 2011). A necessary foundation and enormous challenge for human systems neuroscience is defining the connectome, the complete matrix of structural connections between the nodes of the nervous system, on multiple scales: the macro-connections across the entire brain at the level of centimeters to millimeters, the meso-connections between and within brain areas at the millimeter to micron scale, and the micro-connections between individual neurons at the micron to nanometer resolution (Drobnjak and Alexander, 2011; Swanson and Lichtman, 2016). Tools like magnetic resonance imaging (MRI) offer the spatial range and resolution to image a whole human brain with ~1 mm^3 voxels, whereas electron microscopy (EM) can render the connections between individual neurons, axons, and dendrites with voxels of less than 100 nm^3 – a range spanning four to five orders of magnitude in size.

Currently, no single imaging modality can cover this enormous range of length scales across the *in vivo* or even *ex vivo* human brain. Yet the paramount importance of developing a human imaging tool to begin to explore these structural and connectional motifs across scales has never been more apparent. Basic neuroscience is reaching a stage where alterations in cellular architecture and connectional anatomy are observed in animal models of disease and increasingly in human tissue, both locally and globally, in neuropsychiatric diseases such as autism (Drobnjak et al., 2011; Ianus et al., 2016; Peca et al., 2011; Peca and Feng, 2012) and schizophrenia (Penzes et al., 2011), as well as in the earliest stages of neurodegenerative diseases (Herms and Dorostkar, 2016), in which gross structural alterations are invisible on conventional MRI. The ideal technology for understanding the structural and functional organization of the human brain would integrate across microscopic, mesoscopic, and macroscopic scales and allow for mapping of changes across time (e.g., as a result of neural plasticity, development, and pathology) and between individuals.

Toward this goal, the Connectome 2.0 project targets the development of the next-generation human connectomics and microstructure MRI scanner, tailored for inferring cellular and axonal size and morphology at unprecedented spatial and diffusion resolution throughout the whole brain, while providing greater sensitivity and imaging speed for structural imaging at multiple scales in living human subjects. This transformative advance in imaging the micro-,

meso- and macroscopic structure of the living human brain builds on the experience of engineering the first human MRI scanner equipped with 300 mT/m gradients, the strongest gradients developed for a human scanner to date, which was installed at the Massachusetts General Hospital (MGH) in 2011 as part of the Human Connectome Project (HCP) (Setsompop et al., 2013) and has since been successfully disseminated to at least three other sites worldwide (Jones et al., 2018), as discussed in greater extent in a separate review article included in this special issue (Fan et al., 2021). The original Connectome scanner leveraged such high gradient strengths to enable high-sensitivity, high *b*-value diffusion MRI (dMRI), with the express purpose of mapping the major white matter pathways in the living human brain through diffusion tractography. An important and arguably more impactful byproduct of the original Connectome scanner was the sensitization of *in vivo* dMRI measurements to tissue microstructure at the micron scale (McNab et al., 2013a). The technological advances made by the original HCP have enabled the quantification of the microstructural underpinnings of dMRI contrast in the living human brain, with gains in sensitivity to cellular-level geometry that allow for exploring the biological variability of microstructural parameters within and between individuals, while also relating such parameters to macroscopic connectivity.

Therefore, while the original Connectome scanner has made important contributions to understanding macroscale connectional topology (Fan et al., 2014; Fan et al., 2016), the experience gained over the last decade has demonstrated that dedicated high-gradient performance scanners can also acquire a rich array of dMRI measurements that allow unparalleled *in vivo* assessment of neural tissue microscale structure (Alexander et al., 2017; Jelescu and Budde, 2017; Kiselev, 2017; Lampinen et al., 2019; Novikov et al., 2019; Novikov et al., 2018), such as the relative size and packing density of cells and axons using pulsed gradient and oscillating gradient spin echo sequences (Fan et al., 2020a; Huang et al., 2015; Huang et al., 2020; McNab et al., 2013a; Tax et al., 2020; Veraart et al., 2020; Xu, 2021; Xu et al., 2014) and microscopic anisotropy in gray matter using double diffusion encoding (Jespersen et al., 2013; Shemesh and Cohen, 2011), double oscillating diffusion encoding (Ianus et al., 2017), and free gradient waveforms (Szczepankiewicz et al., 2015), in addition to macro- and mesoscale connectional information. However, the current Connectome instrument remains limited in its ability to resolve the full range of length scales needed to probe the microscopic and mesoscopic structure of the brain, due to basic design limitations, important technical elements, and biological interactions with the large rapidly switching gradients. The experience with the first-generation Connectome scanner and realization of its limitations has motivated an international collaborative multi-site project focused on developing the next-generation human Connectome MRI scanner (Connectome 2.0) to achieve sensitivity to a broader range of cellular and axonal size scales, morphologies, and interconnections represented throughout the brain. Equipped with the lessons on advanced gradient design learned from the initial HCP experience, the Connectome 2.0 project is embarking on a complete redesign of the gradient system to enable ultra-fast slew rate in addition to ultra-high gradient strength. This advance represents a significant technical challenge that is necessary for implementing novel dMRI techniques robustly *in vivo* and gaining sensitivity to the actual range of cellular/axonal sizes and morphologies in the human brain. As the diffusion microstructural metrics

represent inferences of cellular/axonal size and morphology rather than directly imaged quantities, validation of these metrics will be an essential part of this multi-faceted project of technology development.

In this paper, we describe the strategy, planned design and current progress of the Connectome 2.0 scanner and the associated development of advanced acquisition and analysis methods optimized for studying neural tissue microstructure and circuits across multiple length scales in the living human brain. The Connectome 2.0 project will push the limits of sensitivity, resolution, and diffusion-encoding capabilities to unprecedented levels by (1) nearly doubling the current maximum gradient strength (G_{max}) from 300 mT/m to 500 mT/m and tripling the maximum slew rate from 200 T/m/s to 600 T/m/s; (2) designing high-channel count radiofrequency (RF) receive coils and gradient characterization methods to enable maximum sensitivity with greatly reduced artifacts using real-time eddy current corrected dMRI acquisitions; (3) developing new pulse sequences to achieve the highest diffusion- and spatial-resolution ever shown *in vivo*; and (4) calibrating the measurements obtained from this next-generation instrument through systematic validation of the diffusion microstructural metrics in high-fidelity phantoms and *ex vivo* brain tissue at progressively finer scales, and subsequent numerical simulations of diffusion in histology-based substrates. The newfound capabilities of the next-generation Connectome scanner will link an understanding of segregated and distributed *function* with *structural* changes in cortical, subcortical and white matter regions, across spatial scales and relevant behaviors thought to modify brain structure and connectivity in health and disease.

2. Hardware advances for Connectome 2.0

The goal of the original Human Connectome Project was to map the long-range structural connections in the living human brain as comprehensively as possible using diffusion tractography, alongside comprehensive mapping of functional connectivity using functional MRI. To achieve this goal, the first phase of the Human Connectome Project pioneered important advances in MRI hardware and acquisition technology, including ultra-high gradient fields, high-sensitivity receive arrays, and accelerated pulse sequences for achieving whole-brain coverage within scan times feasible for *in vivo* imaging. Many of these technological advances have now made their way into commercially available scanners and have led to dramatic improvements in the spatial, angular, and diffusion resolution that is attainable in the living human brain.

The Connectome 2.0 project will push dMRI technology to the next level by designing a new high-performance gradient package that builds on the success of the original Connectome scanner and encompasses the latest engineering capabilities. To meet the spatial and diffusion resolution goals, the maximal gradient amplitude will be nearly doubled to 500 mT/m, and the speed of the gradients will be accelerated by a factor of three to a maximal slew rate of 600 T/m/s. The performance of the Connectome 2.0 gradient system, as summarized by the product G_{max} · maximum slew rate (Blasche, 2017; Szczepankiewicz et al., 2021), will be at least five times that of the most modern MRI systems available today, including the original Connectome MRI system equipped with G_{max} of 300 mT/m and maximum slew rate of 200 T/m/s.

2.1. Scanner design and choice of field strength

Building on the experience and successful construction of the original MGH Connectome scanner, the Connectome 2.0 scanner is being manufactured in partnership with Siemens on the latest 3T wide-bore scanner, the Vida platform, in keeping with the precedent established at Siemens for embedding the latest gradient technology into state-of-the-art wide bore systems. The choice of 3 Tesla over 7 Tesla for the field strength of the original Connectome scanner was driven by the independence of diffusion contrast on B_0 and the gains in sensitivity from the longer T_2 relaxation times at 3T (Setsompop et al., 2013). Other advantages of performing high-gradient diffusion MRI at 3T include better transmit field homogeneity, decreased vibration and acoustic noise issues, and diminished SAR at 3T compared to 7T.

2.2. Gradient coil design

The design specifications of the Connectome 2.0 gradient coil include a maximum gradient strength of 500 mT/m and slew rate of 600 T/m/s along each gradient axis. To achieve these specifications, an asymmetric head gradient coil design has been chosen. The small inner diameter of the head gradient coil (compared to a conventional whole-body gradient coil) makes for a fundamentally efficient design (Foo et al., 2018, 2020; Winkler et al., 2018), enabling high maximum gradient strength per unit current. Additionally, the head gradient coil has a substantially higher peripheral nerve stimulation (PNS) threshold compared to the whole-body gradient coil used in the original Connectome scanner due to its smaller diameter, which increases the PNS threshold (Lee et al., 2016a; Lee et al., 2016b; Zhang et al., 2003). Furthermore, cardiac stimulation is less of a concern with a head gradient coil compared to a whole-body gradient coil (Schmitt et al., 2012; Zhang et al., 2003) due to the reduced B-field exposure in the torso, which also leads to ~3-fold lower PNS thresholds compared to the whole-body gradient coil used in the original Connectome scanner (Setsompop et al., 2013). The challenges of the head gradient coil design, including cooling, torque/force balancing and effective shielding, are being addressed through a number of advances in gradient coil design that have been made in the last decade since the original Connectome gradient coil was installed.

The Connectome 2.0 head gradient coil design is based on the knowledge gained from the Siemens 7T Impulse head gradient coil (Siemens Healthineers, Erlangen Germany) capable of achieving a maximum gradient strength of 200 mT/m and slew rate of 900 T/m/s per axis when driven with state-of-the-art gradient amplifiers (Feinberg et al., 2021). The small inner diameter of the Connectome 2.0 head gradient coil (44 cm) compared to the whole-body gradient coil used in the original Connectome scanner (gradient coil inner diameter of 61 cm, clear patient bore diameter of 56 cm) enables higher gradient efficiency, i.e., gradient strength per unit current. The higher gradient efficiency of the Connectome 2.0 head gradient coil allows for the use of fewer high-performance gradient amplifiers compared to the original Connectome whole-body gradient coil. Specifically, the Connectome 2.0 gradient system will be driven by six of the latest gradient amplifiers developed by Siemens with a peak current of 1200 A and peak voltage of 2250 V per axis, each of which produces 33% more power than the gradient amplifiers used to drive the

original Connectome whole-body gradient coil (peak current 900 A and peak voltage 2000 V per axis).

The inner bore diameter of 44 cm is relatively large by head gradient coil standards and will accommodate RF coils with many transmit/receive elements, thereby allowing for access to the typical range of human subjects undergoing research scans. The overall geometry of the Impulse head gradient has been adopted with wiring patterns organized in three concentric layers arranged in a stepped fashion to accommodate subjects of varying sizes. The three-layer geometry opens up additional degrees of freedom to minimize vibrations and acoustic noise from Lorentz forces created from the current-carrying wires in the presence of the static magnetic field. For the Connectome 2.0 project, the number and position of windings on each layer have been modified to achieve the target maximum gradient strength of 500 mT/m and slew rate of 600 T/m/s. Direct cooling of the conductor will enable a high current density to be achieved in order to boost gradient performance. Based on the performance of the Impulse gradient, the maximum deviation from linearity of the Connectome 2.0 head gradient is anticipated to be < 10% along each gradient axis. The target specifications of G_{max} = 500 mT/m and maximum slew rate of 600 T/m/s represent the technical limit of what is achievable using the current asymmetric head gradient coil design with an inner diameter of 44 cm.

2.3. Peripheral nerve stimulation

Peripheral nerve stimulation (PNS) is a significant limitation of the maximum usable gradient amplitude and slew rate for the latest generation of high-performance gradient coils. Although most prominent for whole-body gradient coils, PNS is also becoming a significant concern for head gradients (Lee et al., 2016b), (Weiger et al., 2017) (Tan et al., 2019). Therefore, an additional goal in the design phase of the Connectome 2.0 gradient is to minimize PNS propensity.

To achieve this goal, we are leveraging recently developed simulation tools for the accurate prediction of PNS thresholds using realistic whole-body human nerve models in combination with electric field simulations (Davids et al., 2020a, b, 2017, 2019, 2021b). As in the case of the Impulse head gradient (Davids et al., 2021a) (Fig. 1), these PNS modeling methods are being incorporated in the design phase to evaluate different candidate coils and identify design aspects with beneficial impact on PNS thresholds while satisfying the more traditional design specifications. This includes aspects such as coil dimensions, size and linearity of the field of view, as well as the level of coil asymmetry. As in the design phase of the Impulse gradient, the third intermediate winding layer is crucial in providing additional degrees of freedom that can be leveraged to reduce PNS.

After construction of the Connectome 2.0 gradient coil, we will perform an experimental PNS study in healthy human subjects to validate further the PNS modeling tools and assess their value in designing and optimizing high-performance gradient coils. Overall, the PNS simulation tools and experiments offer valuable technology for optimizing the PNS properties of high-performance gradient coils at the design stage.

2.4. Radiofrequency coil design

As part of the Human Connectome Project, a custom 64-channel brain receive-array coil was developed and validated on the original Connectome scanner, which enabled the highest SNR and highest quality accelerated human brain imaging at 3T to date (Keil et al., 2013). Building on the success of this 64-channel coil, a new 72-channel head coil with an integrated field camera is being designed for the Connectome 2.0 scanner, which will combine improved reception sensitivity and dynamic field monitoring to enable distortion-reduced dMRI acquisitions. The 72-channel head coil will offer full coverage of the cerebral hemispheres, cerebellum, and brainstem for optimal assessment of microscale, mesoscale and macroscale connectivity spanning the supratentorial and infratentorial brain (Fig. 2). The limited space inside the Connectome 2.0 scanner's head gradient coil does not allow for a built-in transmit coil, which poses additional challenges to the coil design. Therefore, each receiver array will require its own dedicated local transmit coil to be placed on the patient table.

The original Connectome scanner has demonstrated the potential of a high-gradient strength human MRI scanner to serve as an exquisite platform for *ex vivo* diffusion imaging of human whole brain or hemisphere specimens. In comparison, most preclinical MR imaging systems do not possess the field of view required to image an entire human brain or even a single hemisphere, and those that do provide neither stronger gradient sets nor the requisite number of RF receive channels to use the advanced RF coil technology proposed here. The original Connectome scanner had a 60-channel "panini press" brain slice array coil (Gruber et al., 2014) designed and constructed for imaging of human brain slabs of up to 3 inches in thickness with sufficient sensitivity for single-average high-angular resolution diffusion imaging at 350 μm isotropic resolution using b-values of up to 30,000 s/mm^2 (Wieseotte et al., 2015). The flat geometry of this coil was chosen to provide maximum SNR through a slab of white matter without suffering from depth bias, at the expense of only being able to image a relatively thin slab of the brain, which precludes high-resolution dMRI of the whole brain. In order to map the connectomics of the whole human brain with high spatial resolution, a close-fitting 48-channel *ex vivo* whole brain coil has recently been developed for the original Connectome scanner (Scholz et al., 2021). This array coil enables *ex vivo* whole brain specimens to be imaged at submillimeter spatial resolution with high SNR (see section III.6: *Enabling high spatial resolution diffusion MRI readout for in vivo and ex vivo whole brain microstructural imaging*).

The *ex vivo* imaging capabilities of the Connectome 2.0 scanner will be expanded by constructing a new 64-channel coil capable of holding an entire human brain specimen, similar in construction to the 48-ch *ex vivo* whole brain coil built for the original Connectome scanner (Fig. 3). Due to the comparatively long acquisition times for whole brain *ex vivo* tissue specimens (~34 hours for 550 μm isotropic spatial resolution with 64 diffusion directions and 2 $b = 0$ images, with each imaging volume taking approximately 31.2 minutes to acquire (Ramos-Llorden et al., 2021)), special care will be taken to ensure signal stability over the timeframe of the acquisition. The diffusivity in the *ex vivo* tissue specimen strongly depends on the temperature of the specimen (Roebroeck et al., 2019). The *ex vivo* coil will therefore be constructed to allow control over the specimen temperature

by placing the entire coil setup into a sealed box with a controlled temperature air supply. Temperature control has been shown to be essential for accuracy and reproducibility via the use of temperature stabilized diffusion phantoms (Reischauer et al., 2009) and has been used in recent precision diffusion studies of *ex vivo* tissue in preclinical MRI systems (Bastiani et al., 2016; Teh et al., 2016). Our temperature controlled *ex vivo* coil will similarily ensure the accuracy and reproducibility of dMRI measurements independent of environmental temperature.

2.5. Field monitoring

Since the original design of the Connectome scanner over 10 years ago, magnetic field cameras have become commercially available. Such field cameras enable the monitoring and correction of eddy currents that arise due to interactions between the gradient coil and any conducting structures within the scanner, including the magnet, the gradient coil itself, and the radiofrequency coils. Eddy currents are the dominant cause of image artifacts in dMRI, causing noticeable image distortions even at gradient strengths of 40 mT/m typical for clinical MRI systems. The severity of the artifacts is proportional to the strength of the diffusion-encoding gradient pulses, posing a significant challenge at very high gradient strengths. Therefore, effective eddy current correction approaches will need to be developed for the next-generation Connectome system. So-called gradient pre-emphasis techniques, commonplace in modern MRI machines, significantly reduce the spatially linear eddy current field patterns; however, eddy current fields of higher spatial order are well known (Boesch et al., 1991; Van Vaals and Bergman, 1990) and can neither be compensated nor easily corrected in post-processing. Higher-order eddy current fields with multiple time constants add to the linear encoding gradients and create k-space shifts that vary in space and time. This effect causes the image geometry and resolution to become spatially variable, which is impractical to correct in the image domain.

The Connectome 2.0 scanner will make use of dynamic field monitoring and state-of-the-art image reconstruction techniques that incorporate the monitored field data to maximize the image quality and accuracy of diffusion MRI data measured in the new system (Wilm et al., 2011). Integrated 16-channel clip-on field-cameras (Dietrich et al., 2016) will be incorporated into the 72-channel extended field-of-view coil for *in vivo* imaging and the 64-channel *ex vivo* whole brain coil to allow monitoring of the B_0 and gradient fields simultaneously with the acquisition of *in vivo* and *ex vivo* human brain diffusion data (Wilm et al., 2015). Image reconstruction techniques will be implemented that can model spatially dependent k-space trajectories based on dynamic measurements of the magnetic fields inside the field-of-view. When provided with field measurements of up to 3rd order from the integrated field-cameras embedded in the *in vivo* and *ex vivo* coils, diffusion images with significantly reduced artifacts will be reconstructed (Wilm et al., 2011, 2015). The integration of simultaneous field-camera measurements to provide real-time eddy current information is superior to non-simultaneous field-monitoring approaches as the presence of higher-order, nonlinear eddy current fields combined with significant nonlinear concomitant fields (Bernstein et al., 1998) at high gradient strengths prevent the effective encoding fields from being modeled as a simple linear-time-invariant system. The rise in gradient coil temperature with higher gradient amplitudes (Busch et al., 2014) also breaks the time

invariance property, which further strengthens the need for simultaneous field monitoring. With built-in field-camera monitoring, a new field characterization tailored to the acquisition of each imaging protocol offers a practical and elegant solution and will provide superior image quality to what is currently attainable on the original Connectome system.

The combination of the new high-performance gradient package, a suite of new RF coils for *in vivo* and *ex vivo* imaging, and state-of-the-art field monitoring will result in a significant advance in our ability to acquire diffusion MRI data in the living human brain. Pushing the limits of technically feasible gradient coil engineering and associated hardware advances will enable the exploration of new microstructure properties *in vivo* that thus far could only be measured in *ex vivo* specimens.

3. Advanced acquisition and analysis methods for inferring mesoscopic structure and connectivity in the brain

Diffusion MRI is a unique tool among MR imaging contrasts in that it sheds light on a multitude of microstructural parameters (e.g., cell size, shape and packing density) whose cellular scale dimensions (~μm) are orders of magnitude smaller than the imaged voxel size (~mm). Advanced dMRI techniques hold the most promise among noninvasive methods for probing cellular structure of any depth and location in the living human brain. However, robust methods for *in vivo* mapping of tissue microstructure by dMRI remain elusive due to the demand for fast and strong diffusion-encoding gradients, which has largely limited such studies to region-of-interest analyses in clinical/preclinical MRI systems or *ex vivo* and animal studies on small-bore MRI systems (Alexander, 2008; Alexander et al., 2010; Assaf and Basser, 2005; Assaf et al., 2008; 2004, Barazany et al., 2009; Ferizi et al., 2013; Fieremans et al., 2016; Henriques et al., 2019, 2020; Ianus et al., 2018; Jespersen et al., 2018 2019; Lampinen et al., 2017; Lee et al., 2018;, 2020c; d; Morozov et al., 2013, Nunes et al., 2017, Olesen et al., 2021; Ong and Wehrli, 2010; Ong et al., 2008; Panagiotaki et al., 2012; Stanisz et al., 1997; Szczepankiewicz et al., 2015; Tax et al., 2020; Topgaard, 2017; Veraart et al., 2020; Westin et al., 2016; Zhang et al., 2011).

The availability of higher maximum gradient strength on human MRI scanners has enabled the exploration of these methods within the *in vivo* human brain. Strong gradients of up to 300 mT/m on the current Connectome scanner have enabled axon diameter mapping experiments *in vivo* to a diffusion resolution limit of 3–4 μm (Huang et al., 2015; McNab et al., 2013a; Veraart et al., 2020). The standard pulsed gradient spin echo (PGSE) diffusion sequence has limited sensitivity to compartment size and morphology in heterogeneous tissue microenvironments and is thus limited in capturing the structural diversity of cells in the brain. To access the micron to sub-micron length scale with sufficient sensitivity in the human brain, alternative and complementary approaches are needed, which require higher slew rates as well as high G_{max} to expand the range of gradient waveforms (Topgaard, 2017) that can be played out for *in vivo* human microstructural imaging.

The Connectome 2.0 project will develop a suite of pulse sequences and analyses suited to different types of diffusion encoding for inferring the size, orientation distribution, and multi-scale organization of neurons, glial cells, dendrites and axons in the complex

microenvironment of the human brain. To visualize tissue microstructure within cortical layers to optimal effect, new diffusion acquisition strategies will be developed to enable high spatial resolution whole-brain diffusion MRI readout. The acquisition parameters accessible using the new gradient system will be systematically evaluated against the current range of gradient strengths and diffusion times to achieve an optimal combination of high spatial resolution and high diffusion sensitivity for pushing the envelope on defining mesoscopic (e.g., cortico-cortical connections) and macroscopic connections in the brain.

3.1. Improvements in SNR, echo time and diffusion time

The major benefits of increasing G_{max} to 500 mT/m and maximum slew rate to 600 T/m/s for dMRI are: (1) decreasing the diffusion time Δ needed to achieve the same diffusion-encoding gradient area, (2) shortening the diffusion gradient pulse duration δ and diffusion time Δ to enable probing of diffusion dynamics at shorter timescales and length scales, depending on the context, and (3) shortening the echo time (TE), thereby reducing signal losses from T_2 relaxation. Fig. 4 shows the minimum TE simulated for a standard PGSE diffusion sequence as a function of *b*-value for different maximum gradient strengths. The minimum TE is shown for a gradient strength of 80 mT/m, 300 mT/m, and 500 mT/m. The largest reduction in TE and Δ occurs for high *b*-values. The SNR scales exponentially with TE; therefore, the SNR improvement of the next generation Connectome scanner could be as high as 50% greater than the current system at high *b*-values up to 40,000 s/mm^2, depending on the assumed T_2 relaxation time.

3.2. Shorter diffusion times and axonal beading

The effect of shortening the diffusion time is particularly advantageous for probing tissue microstructure, as shorter diffusion times are expected to sharpen features in the spin probability distribution function (PDF), the mesoscopic distribution of magnetization in tissues, approximately estimated by the Fourier transform of diffusion signals over the diffusion wave vector (Callaghan, 1991). The spin PDF at shorter times retains more mesoscopic details in tissue features, whereas at long times the measured spin PDF is coarse-grained by diffusion and gradually loses the information (Novikov et al., 2019). Furthermore, the near-doubling of G_{max} to 500 mT/m will reduce the resolution limit (~$1/G_{max}^{1/2}$) of cell size by ~23% (Nilsson et al., 2017) and also act synergistically with shorter Δ to shorten the diffusion length ~$(D\Delta)^{1/2}$, subsequently increasing sensitivity to small compartment sizes.

For example, shorter diffusion times may enable the detailed study of the theoretically predicted (Novikov et al., 2014) and recently found (Fieremans et al., 2016; Lee et al., 2020c) $1/\sqrt{t}$ power-law tail in the along-axon diffusion coefficient $D_{\parallel}(t)$, originating from structurally disordered axonal beading. This diffusivity time-dependence along axons has been observed *in vivo* in the major white matter tracts of the human brain (e.g., corpus callosum), where the $D_{\parallel}(t)$ decreases by 3–5% with time t = 20–100 ms (Lee et al., 2020c). Based on the bead distance $\bar{a}$~6 μm along axons reported in the mouse brain (Lee et al., 2020c), the characteristic timescale is roughly $\bar{a}^2/(2D_0)$~6 ms with the intrinsic diffusivity D_0 ~ 3 μm^2/ms. In particular, detecting the crossover between this scaling (t > 20 ms) and the

short-time limit ($t \ll 6$ ms) of $D_{\parallel}(t)$ could robustly pinpoint the beading length scale, which may be a marker for neurodegenerative diseases.

3.3. Effective axonal diameter

Initially, quantifying axon diameter and density was done through approaches such as AxCaliber (Assaf et al., 2008), based on the conventional PGSE sequence applied transverse to major axonal tracts. However, orientation dispersion and axonal undulations (Nilsson et al., 2012), among other effects, confound axonal diameter mapping. Recently, it was suggested that to factor out the axonal orientation dispersion, as well as axonal undulations with wavelengths exceeding the diffusion length, one can employ directional averaging (Jespersen et al., 2013; Kaden et al., 2016; Mollink et al., 2017). The directionally-averaged diffusion signal $\bar{S}(b)$ becomes independent of the orientation dispersion, and in the limit of zero axonal radius, the diffusion MRI signal follows the asymptotic power-law scaling $\bar{S}(b) \sim 1/\sqrt{b}$ at strong diffusion weighting b (McKinnon et al., 2017; Veraart et al., 2019).

The deviation from the $1/\sqrt{b}$ scaling yields an estimate of intra-axonal radial diffusivity and the subsequent effective radius r_{eff} (Veraart et al., 2020). Fig. 5 demonstrates the *in vivo* observation of the power-law scaling of $\bar{S}(b)$ in the brain white matter of two healthy subjects (23–25 years old, female), who underwent imaging on the current Connectome scanner using a custom-built 64-channel head coil. Diffusion measurements using monopolar PGSE were performed with the parameters: diffusion time $\Delta = 27$ ms, gradient pulse duration $\delta = 16$ ms, $b = 1{,}000$–$30{,}000$ s/mm^2, 3 non-diffusion-weighted images (non-DWIs), 32 DWIs of different gradient directions per b-shell, and an additional non-DWI of reversed phase-encoding polarity for correcting susceptibility-induced distortions. The shot-to-shot phase variation in each complex-valued DWI was removed (Eichner et al., 2015), and the real-valued DWIs were processed using the DESIGNER pipeline (Ades-Aron et al., 2018).

Fig. 5 shows that in human brain white matter, the $1/\sqrt{b}$ scaling can be clearly seen at sufficiently high b-value, where the extra-axonal signal is practically suppressed, while the deviation from this power-law scaling that manifests itself via the negative intercept in $b \rightarrow \infty$ limit, provides an estimate of effective radius $r_{\text{eff}} \sim 3$ μm.

Unfortunately, the effective diameter detectable using PGSE even with $G_{\text{max}} = 300$ mT/m is only ~3 μm (Burcaw et al., 2015; Dyrby et al., 2012; Nilsson et al., 2017; Veraart et al., 2020), which is notably larger than the actual diameter of most axons in the brain (~1 μm or less) (Waxman et al., 1995). The proposed gradient system with near-doubling of G_{max} to 500 mT/m and tripling of SLR_{max} to 600 T/m/s will increase the sensitivity of diffusion MRI measurements to a greater proportion of small diameter axons present in the human brain (Fig. 6). While the proposed G_{max} represents the highest achieved to date in a human MRI scanner, it is still lower than what can be achieved in small-bore MR scanners and may thus not be sufficient to provide robust estimation of the smallest axon diameters < 1 μm in the human brain. Nevertheless, we anticipate that the availability of such high gradient strengths may alleviate the bias seen in axon diameter mapping studies performed to date in

human MRI scanners, including the original Connectome MRI scanner, and we look forward to further advances in gradient technology that may help to resolve such biases.

In reality, the orientation of cells and axons varies across the brain, and even the most homogeneous areas of white matter, e.g., corpus callosum, still show some dispersion at the voxel level. To achieve higher sensitivity to cellular and axonal size in the presence of orientation dispersion, oscillating gradient spin echo (OGSE) sequences will be explored for *in vivo* human imaging. OGSE can achieve short effective diffusion times ~1 ms due to the inverse relationship of diffusion time with gradient oscillation frequency (Does et al., 2003; Gore et al., 2010; Xu, 2021; Xu et al., 2014). This is in contradistinction to PGSE, where the diffusion time is limited to > 10 ms by the duration of the 180° refocusing pulse. OGSE has thus far been largely limited to small-bore systems due to the large maximum gradient strength needed to maximize the diffusion-encoding gradient area. Fig. 6 (bottom panel) shows that in the case of dispersed fibers, OGSE may have greater sensitivity for small diameter axons than PGSE under certain conditions. Specifically, low-frequency OGSE is advantageous in cases of unknown fiber direction and/or dispersion because it can achieve high sensitivity to axon diameter at a modest *b*-value, which avoids excessive signal attenuation due to freely diffusing water along the fiber direction (Drobnjak et al., 2016). This is particularly advantageous for systems with high performance gradients, as the area under the diffusion-encoding gradient for OGSE increases with high slew rate. Our redesigned gradient system with stronger G_{max} and increased SLR_{max} will enable OGSE to achieve higher sensitivity to small-diameter cells/axons compared to the current system. Specifically, the simulations in Fig. 6 show that for dispersed fibers, the resolution limit of relatively low-frequency OGSE experiments with 2 to 4 oscillations can be improved from an effective diameter of ~3 to 3.2μm using the current Connectome scanner to ~2.2 to 2.4μm using the target specifications of the Connectome 2.0 scanner. The capability of the Connectome 2.0 scanner to achieve even relatively low oscillation frequencies with stronger gradient amplitudes emphasizes the importance of minimizing PNS for such experiments.

3.4. Gray matter imaging and microscopic anisotropy

Cytoarchitectonic mapping of the human cerebral cortex by dMRI has gained considerable interest in the last few years due to the increased availability and feasibility of performing advanced diffusion-encoding and modeling to map the microanatomical domains of the brain (Fischl and Sereno, 2018; Palombo et al., 2020). Exploring the cellular organization, packing density and orientation of cellular processes within the cortex by dMRI poses several challenges, including the diminished anisotropy observed in cortical gray matter compared to white matter and partial volume effects related to large voxel sizes. Microscopic diffusion anisotropy can be probed using double diffusion encoding (DDE) (Benjamini and Basser, 2014; Benjamini et al., 2020; Cory and Garroway, 1990; Henriques et al., 2021; Komlosh et al., 2007; Lawrenz and Finsterbusch, 2011; Mitra, 1995; Ozarslan, 2009; Shemesh and Cohen, 2011; Shemesh et al., 2010a, b; Yang et al., 2018), double oscillating diffusion encoding (DODE) (Ianus et al., 2017), and *b*-tensor encoding schemes (Afzali et al., 2020; Eriksson et al., 2013; Szczepankiewicz et al., 2015; Topgaard, 2017; Westin et al., 2016) and may enable the distinction of microanatomical domains characterized by randomly oriented compartments of variable size and shape. Previous work

has demonstrated evidence of microscopic anisotropy in human cortical gray matter *in vivo* (Jespersen et al., 2013; Lawrenz and Finsterbusch, 2019; Shemesh and Cohen, 2011; Szczepankiewicz et al., 2015). The ultra-high G_{max} on the Connectome 2.0 system will enable double- and multiple diffusion-encoding periods to be implemented *in vivo* with better SNR than the current Connectome system, providing sensitivity to microscopically oriented domains in gray matter, which have begun to be uncovered with diffusion tensor imaging (McNab et al., 2013b) but remain incompletely characterized with single pulsed field gradient diffusion encoding.

As an initial demonstration of the benefits of high G_{max} for DDE experiments in the living human brain, a fully balanced twice-refocused DDE sequence was designed and optimized for whole brain microscopic anisotropy measurements on the original Connectome scanner. Fig. 7 shows the mean diffusion-weighted images obtained in the whole brain of a healthy volunteer using this DDE sequence. The images were acquired at 2 mm isotropic resolution with each diffusion block having an equal magnitude of q (δ=6 ms, Δ=13 ms, G=226 mT/m, q=0.0395 μm^{-1}, b=800 s/mm^2), separated by a mixing time of 15 ms, with TR/TE=9200/83 ms. A total of 60 directions were acquired following the dPFG-5 scheme (Jespersen et al., 2013) (12 axes of an icosahedron sampled with 5 perpendicular directions for a total of 60 perpendicular encodings) to achieve orientationally invariant estimates of microscopic anisotropy.

As expected, the microscopic anisotropy maps showed relatively uniform values of microscopic anisotropy throughout the white matter regardless of crossing structures. The DDE results also revealed intriguing contrast with higher mean signal intensities in the cerebellum, which is thought to reflect a higher degree of restriction in the tissue microstructural environment. The high degree of restriction observed in the cerebellum corroborates findings obtained with spherical tensor encoding at high b-values (Tax et al., 2020) and may reflect the presence of densely-packed, small granule cells. If corroborated in more individuals, the relevant metrics derived from these experiments could serve as a sensitive probe of cortical architecture by distinguishing areas with different microscopic anisotropy (e.g., randomly arranged ellipsoids representative of cell bodies).

3.5. Other analytic frameworks for multi-scale estimation of brain tissue microstructure

New analytic frameworks are being developed for multi-scale estimation of salient microstructural tissue features, primarily with single and double diffusion encoding paradigms, which are suitable for *in vivo* scanning in humans. These measurements take advantage of the high gradient strengths and slew rates available on the current Connectome scanner and will serve as the foundation for further measurements on the Connectome 2.0 system. The analytic frameworks are being tested and vetted using biomimetic phantoms and *ex vivo* tissue specimens on small-bore scanners at NIH, then migrated to the current Connectome system at MGH for further validation. The analytic approaches encompass both parametric and non-parametric methods, including estimation of the effective axon diameter from mean apparent propagator (MAP) MRI-derived parameters and quantifying microstructural heterogeneity with diffusion tensor distribution (DTD) dMRI. Fig. 8 shows the diffusion time dependence of MAP-MRI and temporal scaling parameters in the human

brain derived from *in vivo* data acquired with the current Connectome scanner (Avram et al., 2021).

The question of whether brain tissue has a self-similar structure that can be represented by fractal exponents remains an open topic of debate, with other work showing short-range disorder implying finite correlation lengths in white matter (Burcaw et al., 2015; Lee et al., 2020c; Novikov et al., 2018). The temporal scaling parameters estimated from the Connectome data include only two diffusion times and are therefore preliminary and should be checked against measurements with a wider range of diffusion times. In general, different microstructure modeling approaches relying on variable assumptions are still very much in need of careful validation, which the Connectome 2.0 is poised to help resolve through comparison of *in vivo* dMRI measurements with those performed in *ex vivo* brain tissue and simulations using realistic tissue substrates derived from electron microscopy (see section IV below).

To capture the complex microstructural organization of brain tissue, the DTD framework has been developed to extract information regarding diffusion anisotropy within the imaging voxel (Magdoom et al., 2021; Westin et al., 2016) by considering a parametrized normal tensor-variate distribution of diffusion tensors. Fig. 9 shows an example of the types of different microstructural "motifs" that can be derived from the covariance of the sub-voxel diffusion tensor distribution obtained from *b*-tensor or DDE measurements. In general, *b*-tensor imaging provides efficient ways of resolving micro-anisotropy and other parameters. DDE, though relatively less efficient, offers measurements of micro-anisotropy in a well-defined diffusion time scale. The DTD analytic framework has been applied to *b*-tensor imaging in the human brain on a clinical scanner (Westin et al., 2016) and is also being applied to DDE measurements on the living human brain using data acquired on the Connectome scanner.

3.6. Enabling high spatial resolution diffusion MRI readout for in vivo and ex vivo whole brain microstructural imaging

To map brain tissue microstructure within gray matter structures and across cortical layers in the living human brain, new diffusion acquisition strategies will be leveraged to enable high spatial resolution whole-brain dMRI readout. The current spatial resolution of dMRI remains low due to inherently low SNR. Indeed, even the highest performing systems used in the Human Connectome Project were only able to achieve 1.25–1.5 mm isotropic resolution with parallel imaging and simultaneous multislice (SMS)/multi-band techniques (Setsompop et al., 2013; Ugurbil et al., 2013). Achieving sub-millimeter resolution with sufficient SNR is critical for capturing the microstructure of different layers within cortex, which is relatively thin (~2–3 mm). gSlider-SMS is a simultaneous multi-slab method that combines a novel "slice dithered" RF slab encoding scheme (Setsompop et al., 2017) with blipped controlled aliasing in parallel imaging (CAIPI) (Setsompop et al., 2012) to enable SNR-efficient whole brain diffusion imaging at voxel sizes as small as 600 μm isotropic. This approach acquires data from 10–15 imaging slices across 2–3 thin slabs to achieve efficient volumetric encoding. Fig. 10 shows how gSlider-SMS acquisition/reconstruction can achieve high SNR efficiency for dMRI of the entire living human brain at 760 μm

isotropic resolution with simultaneous acquisition of 10 slices (Setsompop et al., 2017). This data was acquired on the current Connectome scanner using a custom-built 64-channel head coil and personalized motion-robust stabilizer over a total acquisition time of 15 hours and is being shared as a benchmark dataset exemplifying the unparalleled quality of sub-millimeter resolution dMRI data achievable for *in vivo* acquisitions (Wang et al., 2020, 2021). To achieve distortion-free sub-millimeter diffusion imaging, gSlider-SMS has also been combined with blip-up/down acquisition (BUDA) for multi-shot EPI and dynamic B_0 shimming with a 32-channel AC/DC coil (Liao et al., 2021).

The Connectome 2.0 project will push the limit of slice encoding and simultaneously enable reconstruction methods that enforce smoothness constraints in *k*- and *q*-space to allow subsampled RF and *q*-space encoding (Ramos-Llorden et al., 2020). These advanced readout and image reconstruction methods will accelerate the acquisition by approximately five to seven times while reducing geometric distortion and blurring and will be integrated with the diffusion-encoding methods described in the previous sections.

Tailored acquisition protocols are also being developed for high spatial resolution imaging of *ex vivo* whole human brain specimens that leverage the unique capabilities of the Connectome scanner hardware and advanced *k*-space reconstruction methods. Fig. 11 shows an example of sub-millimeter spatial resolution, high *b*-value dMRI data acquired in a whole postmortem human brain specimen using the dedicated 48-ch whole brain coil (Scholz et al., 2019) described in section II.3. A 3D diffusion-weighted spin-echo multi-shot/segmented EPI sequence (Miller et al., 2011) was played out to achieve a reduced readout duration, enabling reduced distortions and high SNR despite the characteristically short T_2 relaxation time of postmortem brain tissue (Roebroeck et al., 2019). Diffusion-weighted images (730 μm isotropic resolution) encoded with *b*-values of 4000 s/mm^2 and 10 000 s/mm^2 were acquired using the following parameters: TR = 500 ms, TE = 65 ms, echo spacing: 1.22 ms, matrix size = 160 × 268 × 208, field of view 118 × 196 × 152 mm^3, bandwidth = 1244 Hz px^{-1}, 16 shots, EPI factor = 10, no partial Fourier. The phase-encoding direction was anterior-posterior when considering the conventional sagittal plane. Multi-shell diffusion-weighted images were acquired with the following diffusion imaging parameters: b = 4,000 s/mm^2 acquired with 18 non-collinear diffusion-encoding directions and b = 10,000 s/mm^2 acquired with 36 non-collinear diffusion-encoding directions. Images were corrected for eddy current distortions using the eddy tool from the FMRIB Software Library v6.0.

The high spatial resolution afforded by the high sensitivity 48ch whole brain coil and high SNR dMRI acquisition on the Connectome scanner permit imaging of fine-scale structures that remain challenging to visualize with conventional *in vivo* dMRI acquisitions (Fig. 11). The high spatial resolution enables visualization of the gray matter bridges spanning the internal capsule, which shows strong diffusion anisotropy on the colorized FA maps (Fig. 11a). There is clear contrast between the putamen, claustrum, thalamus, globus pallidus, and caudate nucleus in the magnified mean kurtosis map (Fig. 11b). The primary eigenvectors of the diffusion tensor reveal tangential diffusivity in primary somatosensory cortex (S1), in contrast to the adjacent primary motor cortex (M1), in which radial fibers are more prominent (Fig. 11c). The high SNR of the 3D diffusion-weighted acquisition on the current Connectome scanner suggests that even higher spatial resolution may be achieved at high

b-values using the next-generation Connectome scanner and the multi-channel array coils currently under development to enable fitting of more advanced diffusion microstructural models within both superficial and deep white and gray matter regions.

4. Multi-scale validation of microstructural measures in biomimetic phantoms and ex vivo human brain tissue

In order to ensure the widespread use and robust interpretation of the data acquired on this next generation instrument, the diffusion microstructural estimates of tissue properties obtained from dMRI will be calibrated against data obtained from other imaging modalities that have the spatial resolution capable of directly measuring cellular/axonal size, shape and orientation. The Connectome 2.0 project is undertaking a multi-pronged calibration process in which the validity of the biophysical models will be assessed through experiments on custom-made biomimetic tissue phantoms. The microstructural metrics inferred from dMRI measurements performed *in vivo* and on *ex vivo* human brain tissue will also be systematically validated against measurements and numerical simulations taken at progressively higher spatial resolution using micro-CT and EM.

4.1. Validation in biomimetic phantoms

Estimates of axonal size and packing density from dMRI have been debated due to the lack of a gold standard for validation and quality control. To complement the acquisition of never-before accessed *in vivo* diffusion microstructural metrics, we are testing the validity of the biophysical models for inferring cellular and axonal size and orientation against biomimetic tissue phantoms that are custom-made to mimic gray and white matter. A novel taxon (textile water filled tubes) anisotropic diffusion phantom has been constructed to provide “ground truth” verification of the current limits of diffusion imaging and allows for parametric control of diameters, density, and angle dispersion. A recent iteration of the phantom was designed to contain 0.8, 2 and 5 μm inner diameter (ID) tubes with a packing density of 0.5×10^6 per mm^2, scaled to match the range of sizes spanned by myelinated axons in the human brain (Innocenti et al., 2014) and achieving an order of magnitude in reduction of diameter from previous textile-based phantoms (Guise et al., 2016) used for validation of dMRI microstructural measures (Fan et al., 2018). The phantom was scanned on a variety of small- and large-bore systems at three Connectome 2.0 project sites, including the University of Pittsburgh, National Institutes of Health, and Massachusetts General Hospital.

Fig. 12 shows the micro-phantoms and a head-sized 140-mm phantom that contained two test patterns to evaluate variable packing density and crossing angles for comprehensive assessment of fiber geometry and structure on a clinical scanner. Fig. 13 shows the pore diameter distributions estimated from DDE measurements (Benjamini et al., 2014) using the NIH Bruker 7T equipped with a Micro2.5 microimaging probe (G_{max} = 1495 mT/m). Nonparametric fiber diameter distributions of the micro phantoms were estimated from the DDE data based on a previously published analysis pipeline (Benjamini et al., 2016). Peaks were observed in the distributions at 2 and 5 μm ID, in agreement with the expected nominal diameters of the taxon fibers contained within the micro-phantoms. A second

peak in the distribution at 11 μm was thought to reflect the interstitial fluid compartment surrounding the taxons (Komlosh et al., 2018). The results demonstrate the benefits of synthetic, biomimetic phantoms in gaining parametric control over taxon diameters, packing density and orientation, which will be leveraged for systematic multi-scale validation of diffusion microstructural metrics obtained on the next-generation Connectome system.

4.2. Calibration of ex vivo diffusion MRI measurements with micro-CT and EM

The metrics inferred from dMRI measurements in the living human brain will require systematic validation against "gold-standard" measurements taken at progressively finer scales in order to lend confidence to the noninvasive measures of brain tissue microstructure obtained from *in vivo* dMRI. It is important to recognize that a systematic calibration of this scope and level of detail has never been attempted for *in vivo* dMRI measurements, much less on a high-performance system of this caliber. Therefore, we consider the calibration of dMRI measurements obtained on the Connectome 2.0 system to be a necessary and important process that is inextricable from the actual development of the next generation scanner. We expect these efforts to provide a comprehensive set of *in vivo* and *ex vivo* dMRI data obtained in the whole brain and in smaller tissue blocks, with strong correlative data obtained from micro-CT and EM that can be used to test and refine any number of dMRI approaches.

As an initial demonstration of the validation pipeline and insights into brain tissue microstructure provided by such a systematic approach, the Connectome 2.0 project is undertaking a top-down, bottom-up approach to calibrating dMRI measures of axonal microstructure against *ex vivo* dMRI, micro-CT and EM data. In particular, advances in microscopy techniques and accompanying cell segmentation pipelines, along with increases in computational power, have enabled one to perform numerical simulations of diffusion in realistic tissue substrates (Fig. 14), facilitating the validation and optimization of biophysical modeling of dMRI (Andersson et al., 2020; Chin et al., 2002; Lee et al., 2020c, e; Nguyen et al., 2018; Palombo et al., 2019; Xu et al., 2018). For example, previous work has quantitatively analyzed the microstructure in white matter axons, such as the axon diameter distribution, along-axon caliber variation, and orientation dispersion in the mouse corpus callosum using three-dimensional EM (Abdollahzadeh et al., 2019; Lee et al., 2019) and in the macaque brain using synchrotron X-ray nano-holotomography (Andersson et al., 2020). Furthermore, *in silico* diffusion studies in realistic axonal shapes of mouse brain EM have demonstrated that the diffusivity time-dependence along axons is mainly due to caliber variations (Lee et al., 2020c), and that axon size estimation can be confounded by the presence of axonal undulations at the diffusion times achievable on clinical and preclinical systems (Lee et al., 2020b). We have developed an open-source software of diffusion simulations in realistic cell geometries from microscopy data (Fieremans and Lee, 2018; Lee et al., 2020a), providing a universal platform of model validation and protocol optimization for microstructural imaging using dMRI. It is important to keep in mind that *ex vivo* diffusion MRI faces its own challenges in such validation efforts, including the changes in MRI-relevant tissue properties and cell shrinkage incurred by tissue fixation (Roebroeck et al., 2019). Several approaches have been proposed to preserve excised nervous tissue in a viable physiological state that preserves the structural complexity of the tissue (Kakkar et

al., 2018; Richardson et al., 2013) and may be adopted to ensure that the diffusion properties of excised tissue emulate those observed *in vivo* as closely as possible.

With the development of multibeam serial EM (Eberle and Zeidler, 2018), high-resolution images of human white matter now can be acquired at nanometer resolution over volumes of tissue comparable to the MRI voxel size (~mm). The availability of EM data over millimeter-sized volumes would help to obtain representative tissue snapshots of the underlying diffusion MRI physics and to achieve faithful ensemble averaging over all representative microenvironments, as well as providing the capability of studying mesoscopic fluctuations (Burcaw et al., 2015) and biological variability over such length scales. We have estimated histology-based axonal characteristics based on EM images from a sample of human brain tissue obtained from the left temporal lobe in a patient undergoing surgery for removal of an epileptogenic focus in the left hippocampus. Immediately following excision, the tissue sample was placed in glutaraldehyde/paraformaldehyde fixative, stained with reduced osmium tetroxide and embedded in Epon resin (Tapia et al., 2012). The cured block containing full-thickness cerebral cortex and subcortical white matter was trimmed to a 2×3 mm^2 rectangle and a depth of 200 μm and imaged $8 \times 8 \times 30$ nm^3 using serial-section scanning EM (Sigma, Carl Zeiss) with a custom-built automated tape-collecting ultramicrotome (Baena et al., 2019). The subset of images within subcortical white matter (volume of $131 \times 147 \times 39$ μm^3) was extracted from the entire dataset, and the myelinated axons were segmented using supervised deep learning with 3D convolutional neural networks (CNNs) and transfer learning (Tian et al., 2020). Our diffusion simulations in the segmented subcortical white matter axons have demonstrated the predominant contribution of axonal caliber variations to diffusion time-dependence along the length of human axons (Lee et al., 2020e). The established segmentation, characterization and segmentation pipeline will be applied to the entire human white matter EM dataset and new EM and micro-CT datasets with dMRI data acquired on similar tissue samples.

4.3. Validation of macroscale connectional anatomy

The technologies developed as part of the original Connectome project have achieved much higher resolution and SNR than had been previously feasible for *in vivo* dMRI and have laid the groundwork for mapping white matter circuitry with much finer detail. An example of such an advance that has been enabled by Connectome technologies is mapping the topographic organization of small axon bundles within the large pathways of the living human brain. Such topographies had previously been demonstrated by invasive tracer injection studies in non-human primates (Heilbronner and Haber, 2014; Lehman et al., 2011). The *in vivo* human dMRI scans that were widely available prior to the development of the original Connectome scanner, while sufficient for mapping the large highways of the brain, are not suitable for replicating the topographic organization of small axon bundles within these highways. However, the MGH-USC Human Connectome Project datasets (Fan et al., 2016) have been shown to be capable of replicating these detailed topographies (Safadi et al., 2018), thanks to their high spatial resolution and SNR. Furthermore, comparisons of ground truth axonal orientations from optical imaging to diffusion orientations from data collected on *ex vivo* human brain samples in a preclinical 9.4T system suggest that high spatial resolution (1 mm isotropic voxel size or smaller)

has an even greater impact than high angular resolution in resolving complex fiber configurations (Jones et al., 2020). Thus, we anticipate that the next-generation Connectome scanner, which will allow us to achieve sub-mm spatial resolution in the entire living human brain while enhancing contrast-to-noise ratio, will increase the accuracy of mapping the fine topographical organization of white matter pathways *in vivo*.

The principles of topographic fidelity and microstructural specificity point the way toward refining our view of macroscale connectivity in the human brain, by bringing together all of the tools for mapping of micro-, meso- and macroscale connectional anatomy developed as part of the Connectome 2.0 project. For more information on the validation of information on connectional anatomy obtained from dMRI, and to ensure that these new technologies are enhancing its accuracy, we refer the reader to the detailed review article included in this special issue (Yendiki, 2021).

5. Conclusion

Our goal here is to translate our initial experience with the original Connectome scanner into building a one-of-a-kind high-slew rate, ultra-high-gradient strength MRI scanner that is optimized for the study of gray and white matter microstructure and connectional anatomy across multiple length scales. By greatly enhancing the slew rate, we will achieve shorter effective diffusion times needed to probe micron-sized structures within the imaging voxel. By increasing the maximum gradient strength and overall SNR, we push the diffusion connectional resolution and sensitivity to the level needed to map regional cortico-cortical connectivity. Calibration of our diffusion measurements of neuronal and axonal structure in living human beings against *ex vivo* measurements obtained with appropriately scaled gold standard measurements will be essential to delivering a tool that is robust to interpretation and can be readily applied to study variations within and between individuals. Through this multi-faceted project of technology development and validation, we envision creating the next generation diffusion MRI scanner capable of imaging the complex architecture and structural basis of brain function across multiple scales.

Acknowledgments

We gratefully acknowledge Dr. Bruce Fischl for helpful discussions in the formulation of this work. We thank Ms. Maya Polackal for assistance in volunteer recruitment and data collection. This work was supported by the National Institutes of Health (grant numbers U01-EB026996, U01-EB025162, P41-EB030006, R01-EB028797, R01-HL131635, K23-NS096056, P41-EB017183, R01-NS088040, R01-NS118187).

Data and code availability:

The data and code from this study will be made available upon reasonable request.

References

Abdollahzadeh A, Belevich I, Jokitalo E, Tohka J, Sierra A, 2019. Automated 3D axonal morphometry of white matter. Sci. Rep. 9, 6084. [PubMed: 30988411]

Ades-Aron B, Veraart J, Kochunov P, McGuire S, Sherman P, Kellner E, Novikov DS, Fieremans E, 2018. Evaluation of the accuracy and precision of the diffusion parameter EStImation with Gibbs and NoisE removal pipeline. Neuroimage 183, 532–543. [PubMed: 30077743]

Afzali M, Aja-Fernandez S, Jones DK, 2020. Direction-averaged diffusion-weighted MRI signal using different axisymmetric B-tensor encoding schemes. Magn. Reson. Med. 84, 1579–1591. [PubMed: 32080890]

Alexander DC, 2008. A general framework for experiment design in diffusion MRI and its application in measuring direct tissue-microstructure features. Magn. Reson. Med. 60, 439–448. [PubMed: 18666109]

Alexander DC, Dyrby TB, Nilsson M, Zhang H, 2017. Imaging brain microstructure with diffusion MRI: practicality and applications. NMR Biomed..

Alexander DC, Hubbard PL, Hall MG, Moore EA, Ptito M, Parker GJ, Dyrby TB, 2010. Orientationally invariant indices of axon diameter and density from diffusion MRI. Neuroimage 52, 1374–1389. [PubMed: 20580932]

Andersson M, Kjer HM, Rafael-Patino J, Pacureanu A, Pakkenberg B, Thiran JP, Ptito M, Bech M, Bjorholm Dahl A, Andersen Dahl V, Dyrby TB, 2020. Axon morphology is modulated by the local environment and impacts the noninvasive investigation of its structure-function relationship. Proc. Natl. Acad. Sci. U. S. A. 117, 33649–33659. [PubMed: 33376224]

Assaf Y, Basser PJ, 2005. Composite hindered and restricted model of diffusion (CHARMED) MR imaging of the human brain. Neuroimage 27, 48–58. [PubMed: 15979342]

Assaf Y, Blumenfeld-Katzir T, Yovel Y, Basser PJ, 2008. AxCaliber: a method for measuring axon diameter distribution from diffusion MRI. Magn. Reson. Med. 59, 1347–1354. [PubMed: 18506799]

Assaf Y, Freidlin RZ, Rohde GK, Basser PJ, 2004. New modeling and experimental framework to characterize hindered and restricted water diffusion in brain white matter. Magn. Reson. Med. 52, 965–978. [PubMed: 15508168]

Avram AV, Sarlls JE, Barnett AS, Özarslan E, Thomas C, Irfanoglu MO, Hutchinson E, Pierpaoli C, Basser PJ, 2016. Clinical feasibility of using mean apparent propagator (MAP) MRI to characterize brain tissue microstructure. Neuroimage 127, 422–434. [PubMed: 26584864]

Avram AV, Tian Q, Fan Q, Huang SY, Basser PJ, 2021. The diffusion time dependence of MAP-MRI parameters in the human brain. Proc. Intl. Soc. Mag. Reson. Med. 29, 2465.

Baena V, Schalek RL, Lichtman JW, Terasaki M, 2019. Serial-section electron microscopy using automated tape-collecting ultramicrotome (ATUM). Methods Cell Biol. 152, 41–67. [PubMed: 31326026]

Barazany D, Basser PJ, Assaf Y, 2009. In vivo measurement of axon diameter distribution in the corpus callosum of rat brain. Brain 132, 1210–1220. [PubMed: 19403788]

Bastiani M, Oros-Peusquens AM, Seehaus A, Brenner D, Mollenhoff K, Celik A, Felder J, Bratzke H, Shah NJ, Galuske R, Goebel R, Roebroeck A, 2016. Automatic segmentation of human cortical layer-complexes and architectural areas using ex vivo diffusion MRI and its validation. Front. Neurosci. 10, 487. [PubMed: 27891069]

Benjamini D, Basser PJ, 2014. Joint radius-length distribution as a measure of anisotropic pore eccentricity: an experimental and analytical framework. J. Chem. Phys. 141, 214202. [PubMed: 25481136]

Benjamini D, Hutchinson EB, Komlosh ME, Comrie CJ, Schwerin SC, Zhang G, Pierpaoli C, Basser PJ, 2020. Direct and specific assessment of axonal injury and spinal cord microenvironments using diffusion correlation imaging. Neuroimage 221, 117195. [PubMed: 32726643]

Benjamini D, Komlosh ME, Basser PJ, Nevo U, 2014. Nonparametric pore size distribution using d-PFG: comparison to s-PFG and migration to MRI. J. Magn. Reson. 246, 36–45. [PubMed: 25064269]

Benjamini D, Komlosh ME, Holtzclaw LA, Nevo U, Basser PJ, 2016. White matter microstructure from nonparametric axon diameter distribution mapping. Neuroimage 135, 333–344. [PubMed: 27126002]

Bernstein MA, Zhou XJ, Polzin JA, King KF, Ganin A, Pelc NJ, Glover GH, 1998. Concomitant gradient terms in phase contrast MR: analysis and correction. Magn. Reson. Med. 39, 300–308. [PubMed: 9469714]

Blasche M, 2017. Gradient performance and gradient amplifier power. MAGNETOM Flash, Siemens Healthcare 69.

Boesch C, Gruetter R, Martin E, 1991. Temporal and spatial analysis of fields generated by eddy currents in superconducting magnets: optimization of corrections and quantitative characterization of magnet/gradient systems. Magn. Reson. Med. 20, 268–284. [PubMed: 1775052]

Burcaw LM, Fieremans E, Novikov DS, 2015. Mesoscopic structure of neuronal tracts from time-dependent diffusion. Neuroimage 114, 18–37. [PubMed: 25837598]

Busch J, Vannesjo SJ, Barmet C, Pruessmann KP, Kozerke S, 2014. Analysis of temperature dependence of background phase errors in phase-contrast cardiovascular magnetic resonance. J. Cardiovasc. Magn. Reson. 16, 97. [PubMed: 25497004]

Callaghan PT, 1991. Principles of Nuclear Magnetic Resonance Microscopy. Oxford University Press, Oxford.

Chin CL, Wehrli FW, Hwang SN, Takahashi M, Hackney DB, 2002. Biexponential diffusion attenuation in the rat spinal cord: computer simulations based on anatomic images of axonal architecture. Magn. Reson. Med. 47, 455–460. [PubMed: 11870831]

Cory DG, Garroway AN, 1990. Measurement of translational displacement probabilities by NMR: an indicator of compartmentation. Magn. Reson. Med. 14, 435–444. [PubMed: 2355827]

Davids M, Dietz P, Ruyters G, Roesler M, Klein V, Guerin B, Feinberg D, Wald LL, 2021a. PNS optimization of a high-performance asymmetric gradient coil for head imaging. In: Proceedings of the 29th Annual Meeting of the ISMRM., Virtual Meeting.

Davids M, Guerin B, Klein V, Schmelz M, Schad LR, Wald LL, 2020a. Optimizing selective stimulation of peripheral nerves with arrays of coils or surface electrodes using a linear peripheral nerve stimulation metric. J. Neural Eng. 17, 016029. [PubMed: 31665707]

Davids M, Guerin B, Klein V, Wald LL, 2020b. Optimization of MRI gradient coils with explicit peripheral nerve stimulation constraints. IEEE Trans Med Imaging PP.

Davids M, Guérin B, Malzacher M, Schad LR, Wald LL, 2017. Predicting magnetostimulation thresholds in the peripheral nervous system using realistic body models. Sci. Rep. 7, 5316. [PubMed: 28706244]

Davids M, Guerin B, Vom Endt A, Schad LR, Wald LL, 2019. Prediction of peripheral nerve stimulation thresholds of MRI gradient coils using coupled electromagnetic and neurodynamic simulations. Magn. Reson. Med. 81, 686–701. [PubMed: 30094874]

Davids M, Guerin B, Wald LL, 2021b. A Huygens' surface approach to rapid characterization of Peripheral Nerve Stimulation (PNS). Magn. Reson. Med..

Dietrich BE, Brunner DO, Wilm BJ, Barmet C, Gross S, Kasper L, Haeberlin M, Schmid T, Vannesjo SJ, Pruessmann KP, 2016. A field camera for MR sequence monitoring and system analysis. Magn. Reson. Med. 75, 1831–1840. [PubMed: 25975352]

Does MD, Parsons EC, Gore JC, 2003. Oscillating gradient measurements of water diffusion in normal and globally ischemic rat brain. Magn. Reson. Med. 49, 206–215. [PubMed: 12541239]

Drobnjak I, Alexander DC, 2011. Optimising time-varying gradient orientation for microstructure sensitivity in diffusion-weighted MR. J. Magn. Reson. 212, 344–354. [PubMed: 21889378]

Drobnjak I, Siow B, Alexander DC, 2010. Optimizing gradient waveforms for microstructure sensitivity in diffusion-weighted MR. J. Magn. Reson. 206, 41–51. [PubMed: 20580294]

Drobnjak I, Zhang H, Hall MG, Alexander DC, 2011. The matrix formalism for generalised gradients with time-varying orientation in diffusion NMR. J. Magn. Reson. 210, 151–157. [PubMed: 21435926]

Drobnjak I, Zhang H, Ianus A, Kaden E, Alexander DC, 2016. PGSE, OGSE, and sensitivity to axon diameter in diffusion MRI: Insight from a simulation study. Magn. Reson. Med. 75, 688–700. [PubMed: 25809657]

Dyrby TB, Sogaard LV, Hall MG, Ptito M, Alexander DC, 2012. Contrast and stability of the axon diameter index from microstructure imaging with diffusion MRI. Magn. Reson. Med..

Eberle AL, Zeidler D, 2018. Multi-beam scanning electron microscopy for high-throughput imaging in connectomics research. Front Neuroanat 12, 112. [PubMed: 30618653]

Eichner C, Cauley SF, Cohen-Adad J, Moller HE, Turner R, Setsompop K, Wald LL, 2015. Real diffusion-weighted MRI enabling true signal averaging and increased diffusion contrast. Neuroimage 122, 373–384. [PubMed: 26241680]

Eriksson S, Lasic S, Topgaard D, 2013. Isotropic diffusion weighting in PGSE NMR by magic-angle spinning of the q-vector. J. Magn. Reson. 226, 13–18. [PubMed: 23178533]

Fan Q, Eichner C, Afzali M, Mueller L, Tax CMW, Davids M, Mahmutovic M, Keil B, Bilgic B, Setsompop K, Lee HH, Tian Q, Maffei C, Yendiki A, Song YQ, Huang CC, Lin CP, Weiskopf N, Anwander A, Jones DK, Rosen BR, Wald LL, Huang SY, 2021. Mapping the Human Connectome Using Diffusion MRI at 300 mT/m Gradient Strength: Methodological Advances and Scientific Impact. Neuroimage Submitted for publication.

Fan Q, Nummenmaa A, Wichtmann B, Witzel T, Mekkaoui C, Schneider W, Wald LL, Huang SY, 2018. Validation of diffusion MRI estimates of compartment size and volume fraction in a biomimetic brain phantom using a human MRI scanner with 300mT/m maximum gradient strength. Neuroimage 182, 469–478. [PubMed: 29337276]

Fan Q, Nummenmaa A, Witzel T, Ohringer N, Tian Q, Setsompop K, Klawiter EC, Rosen BR, Wald LL, Huang SY, 2020a. Axon diameter index estimation independent of fiber orientation distribution using high-gradient diffusion MRI. Neuroimage 222, 117197. [PubMed: 32745680]

Fan Q, Nummenmaa A, Witzel T, Zanzonico R, Keil B, Cauley S, Polimeni JR, Tisdall D, Van Dijk KR, Buckner RL, Wedeen VJ, Rosen BR, Wald LL, 2014. Investigating the capability to resolve complex white matter structures with high b–value diffusion magnetic resonance imaging on the MGH-USC Connectom scanner. Brain Connect. 4, 718–726. [PubMed: 25287963]

Fan Q, Witzel T, Nummenmaa A, Van Dijk KR, Van Horn JD, Drews MK, Somerville LH, Sheridan MA, Santillana RM, Snyder J, Hedden T, Shaw EE, Hollinshead MO, Renvall V, Zanzonico R, Keil B, Cauley S, Polimeni JR, Tisdall D, Buckner RL, Wedeen VJ, Wald LL, Toga AW, Rosen BR, 2016. MGH-USC Human Connectome Project datasets with ultra-high b-value diffusion MRI. Neuroimage 124, 1108–1114. [PubMed: 26364861]

Fan Q, Witzel T, Tounekti S, Tian Q, Ngamsombat C, Polackal M, Nummenmaa A, Huang SY, 2020b. Investigating restricted diffusion within different cortical regions using double-diffusion encoding. Int. Soc. Magn. Reson. Med..

Feinberg D, Dietz P, Liu C, Setsompop K, Mukherjee P, Wald LL, Vu AT, Beckett A, Gonzalez Insua I, Schroeder M, Stocker S, Bell PH, Rummert E, Davids M, 2021. Design and development of a next-generation 7T human brain scanner with high-performance gradient coil and dense RF arrays. In: Proceedings of the 29th Annual Meeting of the ISMRM, Virtual Meeting.

Ferizi U, Schneider T, Tariq M, Wheeler-Kingshott CA, Zhang H, Alexander DC, 2013. The importance of being dispersed: a ranking of diffusion MRI models for fibre dispersion using in vivo human brain data. Med. Image Comput. Comput. Assist. Interv. 16, 74–81.

Fieremans E, Burcaw LM, Lee HH, Lemberskiy G, Veraart J, Novikov DS, 2016. In vivo observation and biophysical interpretation of time-dependent diffusion in human white matter. Neuroimage 129, 414–427. [PubMed: 26804782]

Fieremans E, Lee HH, 2018. Physical and numerical phantoms for the validation of brain microstructural MRI: a cookbook. Neuroimage 182, 39–61. [PubMed: 29920376]

Fischl B, Sereno MI, 2018. Microstructural parcellation of the human brain. Neuroimage 182, 219–231. [PubMed: 29496612]

Foo TKF, Laskaris E, Vermilyea M, Xu M, Thompson P, Conte G, Van Epps C, Immer C, Lee SK, Tan ET, Graziani D, Mathieu JB, Hardy CJ, Schenck JF, Fiveland E, Stautner W, Ricci J, Piel J, Park K, Hua Y, Bai Y, Kagan A, Stanley D, Weavers PT, Gray E, Shu Y, Frick MA, Campeau NG, Trzasko J, Huston J 3rd, Bernstein MA, 2018. Lightweight, compact, and high-performance 3T MR system for imaging the brain and extremities. Magn Reson Med 80, 2232–2245. [PubMed: 29536587]

Foo TKF, Tan ET, Vermilyea ME, Hua Y, Fiveland EW, Piel JE, Park K, Ricci J, Thompson PS, Graziani D, Conte G, Kagan A, Bai Y, Vasil C, Tarasek M, Yeo DTB, Snell F, Lee D, Dean A, DeMarco JK, Shih RY, Hood MN, Chae H, Ho VB, 2020. Highly efficient head-only magnetic field insert gradient coil for achieving simultaneous high gradient amplitude and slew rate at 3.0T (MAGNUS) for brain microstructure imaging. Magn Reson Med 83, 2356–2369. [PubMed: 31763726]

Gore JC, Xu J, Colvin DC, Yankeelov TE, Parsons EC, Does MD, 2010. Characterization of tissue structure at varying length scales using temporal diffusion spectroscopy. NMR Biomed. 23, 745–756. [PubMed: 20677208]

Gruber B, Keil B, Witzel T, Nummenmaa A, Wald LL, 2014. A 60-channel ex-vivo brain-slice coil array for 3T imaging. In: Proceedings of the 22nd Annual Meeting of the ISMRM., Milan, Italy, p. 4885.

Guise C, Fernandes MM, Nobrega JM, Pathak S, Schneider W, Fangueiro R, 2016. Hollow polypropylene yarns as a biomimetic brain phantom for the validation of high-definition fiber tractography imaging. ACS Appl. Mater. Interfaces 8, 29960–29967. [PubMed: 27723307]

Heilbronner SR, Haber SN, 2014. Frontal cortical and subcortical projections provide a basis for segmenting the cingulum bundle: implications for neuroimaging and psychiatric disorders. J. Neurosci. 34, 10041–10054. [PubMed: 25057206]

Henriques RN, Jespersen SN, Shemesh N, 2019. Microscopic anisotropy misestimation in spherical-mean single diffusion encoding MRI. Magn. Reson. Med. 81, 3245–3261. [PubMed: 30648753]

Henriques RN, Jespersen SN, Shemesh N, 2020. Correlation tensor magnetic resonance imaging. Neuroimage 211, 116605. [PubMed: 32044435]

Henriques RN, Palombo M, Jespersen SN, Shemesh N, Lundell H, Ianus A, 2021. Double diffusion encoding and applications for biomedical imaging. J. Neurosci. Methods 348, 108989. [PubMed: 33144100]

Herms J, Dorostkar MM, 2016. Dendritic spine pathology in neurodegenerative diseases. Annu. Rev. Pathol. 11, 221–250. [PubMed: 26907528]

Huang SY, Nummenmaa A, Witzel T, Duval T, Cohen-Adad J, Wald LL, McNab JA, 2015. The impact of gradient strength on in vivo diffusion MRI estimates of axon diameter. Neuroimage 106, 464–472. [PubMed: 25498429]

Huang SY, Tian Q, Fan Q, Witzel T, Wichtmann B, McNab JA, Daniel Bireley J, Machado N, Klawiter EC, Mekkaoui C, Wald LL, Nummenmaa A, 2020. High-gradient diffusion MRI reveals distinct estimates of axon diameter index within different white matter tracts in the in vivo human brain. Brain Struct. Funct. 225, 1277–1291. [PubMed: 31563995]

Ianus A, Drobnjak I, Alexander DC, 2016. Model-based estimation of microscopic anisotropy using diffusion MRI: a simulation study. NMR Biomed. 29, 672–685. [PubMed: 27003223]

Ianus A, Jespersen SN, Serradas Duarte T, Alexander DC, Drobnjak I, Shemesh N, 2018. Accurate estimation of microscopic diffusion anisotropy and its time dependence in the mouse brain. Neuroimage 183, 934–949. [PubMed: 30145206]

Ianus A, Shemesh N, Alexander DC, Drobnjak I, 2017. Double oscillating diffusion encoding and sensitivity to microscopic anisotropy. Magn. Reson. Med. 78, 550–564. [PubMed: 27580027]

Ianus A, Siow B, Drobnjak I, Zhang H, Alexander DC, 2013. Gaussian phase distribution approximations for oscillating gradient spin echo diffusion MRI. J. Magn. Reson. 227, 25–34. [PubMed: 23261952]

Innocenti GM, Vercelli A, Caminiti R, 2014. The diameter of cortical axons depends both on the area of origin and target. Cereb. Cortex 24, 2178–2188. [PubMed: 23529006]

Jelescu IO, Budde MD, 2017. Design and validation of diffusion MRI models of white matter. Front. Phys 28.

Jespersen SN, Lundell H, Sonderby CK, Dyrby TB, 2013. Orientationally invariant metrics of apparent compartment eccentricity from double pulsed field gradient diffusion experiments. NMR Biomed. 26, 1647–1662. [PubMed: 24038641]

Jespersen SN, Olesen JL, Hansen B, Shemesh N, 2018. Diffusion time dependence of microstructural parameters in fixed spinal cord. Neuroimage 182, 329–342. [PubMed: 28818694]

Jespersen SN, Olesen JL, Ianus A, Shemesh N, 2019. Effects of nongaussian diffusion on “isotropic diffusion” measurements: an ex-vivo microimaging and simulation study. J. Magn. Reson. 300, 84–94. [PubMed: 30711786]

Jones DK, Alexander DC, Bowtell R, Cercignani M, Dell’Acqua F, McHugh DJ, Miller KL, Palombo M, Parker GJM, Rudrapatna US, Tax CMW, 2018. Microstructural imaging of the human brain with a ‘super-scanner’: 10 key advantages of ultra-strong gradients for diffusion MRI. Neuroimage 182, 8–38. [PubMed: 29793061]

Jones R, Grisot G, Augustinack J, Magnain C, Boas DA, Fischl B, Wang H, Yendiki A, 2020. Insight into the fundamental trade-offs of diffusion MRI from polarization-sensitive optical coherence tomography in ex vivo human brain. Neuroimage 214, 116704. [PubMed: 32151760]

Kaden E, Kruggel F, Alexander DC, 2016. Quantitative mapping of the per-axon diffusion coefficients in brain white matter. Magn. Reson. Med. 75, 1752–1763. [PubMed: 25974332]

Kakkar LS, Bennett OF, Siow B, Richardson S, Ianus A, Quick T, Atkinson D, Phillips JB, Drobnjak I, 2018. Low frequency oscillating gradient spin-echo sequences improve sensitivity to axon diameter: an experimental study in viable nerve tissue. Neuroimage 182, 314–328. [PubMed: 28774648]

Keil B, Blau JN, Biber S, Hoecht P, Tountcheva V, Setsompop K, Triantafyllou C, Wald LL, 2013. A 64-channel 3T array coil for accelerated brain MRI. Magn Reson Med 70, 248–258. [PubMed: 22851312]

Kiselev VG, 2017. Fundamentals of diffusion MRI physics. NMR Biomed. 30.

Komlosh ME, Benjamini D, Hutchinson EB, King S, Haber M, Avram AV, Holtzclaw LA, Desai A, Pierpaoli C, Basser PJ, 2018. Using double pulsed-field gradient MRI to study tissue microstructure in traumatic brain injury (TBI). Microporous Mesoporous Mater. 269, 156–159. [PubMed: 30337835]

Komlosh ME, Horkay F, Freidlin RZ, Nevo U, Assaf Y, Basser PJ, 2007. Detection of microscopic anisotropy in gray matter and in a novel tissue phantom using double Pulsed Gradient Spin Echo MR. J. Magn. Reson. 189, 38–45. [PubMed: 17869147]

Lampinen B, Szczepankiewicz F, Martensson J, van Westen D, Sundgren PC, Nilsson M, 2017. Neurite density imaging versus imaging of microscopic anisotropy in diffusion MRI: a model comparison using spherical tensor encoding. Neuroimage 147, 517–531. [PubMed: 27903438]

Lampinen B, Szczepankiewicz F, Noven M, van Westen D, Hansson O, Englund E, Martensson J, Westin CF, Nilsson M, 2019. Searching for the neurite density with diffusion MRI: challenges for biophysical modeling. Hum. Brain Mapp. 40, 2529–2545. [PubMed: 30802367]

Lawrenz M, Finsterbusch J, 2011. Detection of microscopic diffusion anisotropy on a whole-body MR system with double wave vector imaging. Magn. Reson. Med. 66, 1405–1415. [PubMed: 21488098]

Lawrenz M, Finsterbusch J, 2019. Detection of microscopic diffusion anisotropy in human cortical gray matter in vivo with double diffusion encoding. Magn. Reson. Med. 81, 1296–1306. [PubMed: 30206991]

Lee H-H, Yaros K, Veraart J, Pathan JL, Liang F-X, Kim SG, Novikov DS, Fieremans E, 2019. Along-axon diameter variation and axonal orientation dispersion revealed with 3D electron microscopy: implications for quantifying brain white matter microstructure with histology and diffusion MRI. Brain Struct. Funct. 224, 1469–1488. [PubMed: 30790073]

Lee HH, Fieremans E, Novikov DS, 2018. What dominates the time dependence of diffusion transverse to axons: Intra- or extra-axonal water? Neuroimage 182, 500–510. [PubMed: 29253652]

Lee HH, Fieremans E, Novikov DS, 2020a. Realistic Microstructure Simulator (RMS): Monte Carlo simulations of diffusion in three-dimensional cell segmentations of microscopy images. J. Neurosci. Methods 350, 109018. [PubMed: 33279478]

Lee HH, Jespersen SN, Fieremans E, Novikov DS, 2020b. The impact of realistic axonal shape on axon diameter estimation using diffusion MRI. Neuroimage 223, 117228. [PubMed: 32798676]

Lee HH, Papaioannou A, Kim SL, Novikov DS, Fieremans E, 2020c. A time-dependent diffusion MRI signature of axon caliber variations and beading. Commun. Biol..

Lee HH, Papaioannou A, Novikov DS, Fieremans E, 2020d. In vivo observation and biophysical interpretation of time-dependent diffusion in human cortical gray matter. Neuroimage 222, 117054. [PubMed: 32585341]

Lee HH, Tian Q, Ngamsombat C, Berger DR, Lichtman JW, Huang SY, Novikov DS, Fieremans E, 2020e. Random walk simulations of diffusion in human brain white matter from 3d EM validate diffusion time-dependence transverse and parallel to axons. Proc. Intl. Soc. Mag. Reson. Med. 28.

Lee SK, Mathieu JB, Graziani D, Piel J, Budesheim E, Fiveland E, Hardy CJ, Tan ET, Amm B, Foo TK, Bernstein MA, Huston J 3rd, Shu Y, Schenck JF, 2016a. Peripheral nerve stimulation characteristics of an asymmetric head-only gradient coil compatible with a high-channel-count receiver array. Magn. Reson. Med. 76, 1939–1950. [PubMed: 26628078]

Lee SK, Mathieu JB, Graziani D, Piel J, Budesheim E, Fiveland E, Hardy CJ, Tan ET, Amm B, Foo TKF, 2016b. Peripheral nerve stimulation characteristics of an asymmetric head-only gradient

coil compatible with a high-channel-count receiver array. Magn. Reson. Med. 76, 1939–1950. [PubMed: 26628078]

Lehman JF, Greenberg BD, McIntyre CC, Rasmussen SA, Haber SN, 2011. Rules ventral prefrontal cortical axons use to reach their targets: implications for diffusion tensor imaging tractography and deep brain stimulation for psychiatric illness. J. Neurosci. 31, 10392–10402. [PubMed: 21753016]

Liao C, Bilgic B, Tian Q, Stockmann JP, Cao X, Fan Q, Iyer SS, Wang F, Ngamsombat C, Lo WC, Manhard MK, Huang SY, Wald LL, Setsompop K, 2021. Distortion-free, high-isotropic-resolution diffusion MRI with gSlider BUDA-EPI and multicoil dynamic B0 shimming. Magn. Reson. Med..

Lichtman JW, Denk W, 2011. The big and the small: challenges of imaging the brain's circuits. Science 334, 618–623. [PubMed: 22053041]

Magdoom KN, Pajevic S, Dario G, Basser PJ, 2021. A new framework for MR diffusion tensor distribution. Sci. Rep. 11, 2766. [PubMed: 33531530]

McKinnon ET, Jensen JH, Glenn GR, Helpern JA, 2017. Dependence on b-value of the direction-averaged diffusion-weighted imaging signal in brain. Magn. Reson. Imaging 36, 121–127. [PubMed: 27989904]

McNab JA, Edlow BL, Witzel T, Huang SY, Bhat H, Heberlein K, Feiweier T, Liu K, Keil B, Cohen-Adad J, Tisdall MD, Folkerth RD, Kinney HC, Wald LL, 2013a. The Human Connectome Project and beyond: initial applications of 300 mT/m gradients. Neuroimage 80, 234–245. [PubMed: 23711537]

McNab JA, Polimeni JR, Wang R, Augustinack JC, Fujimoto K, Stevens A, Triantafyllou C, Janssens T, Farivar R, Folkerth RD, Vanduffel W, Wald LL, 2013b. Surface based analysis of diffusion orientation for identifying architectonic domains in the in vivo human cortex. Neuroimage 69, 87–100. [PubMed: 23247190]

Miller KL, Stagg CJ, Douaud G, Jbabdi S, Smith SM, Behrens TEJ, Jenkinson M, Chance SA, Esiri MM, Voets NL, Jenkinson N, Aziz TZ, Turner MR, Johansen-Berg H, McNab JA, 2011. Diffusion imaging of whole, post-mortem human brains on a clinical MRI scanner. Neuroimage 57, 167–181. [PubMed: 21473920]

Mitra PP, 1995. Multiple wave-vector extensions of the NMR pulsed-field-gradient spin-echo diffusion measurement. Phys. Rev. B 51, 15074–15078.

Mollink J, Kleinnijenhuis M, Cappellen van Walsum AV, Sotiropoulos SN, Cottaar M, Mirfin C, Heinrich MP, Jenkinson M, Pallebage-Gamarallage M, Ansorge O, Jbabdi S, Miller KL, 2017. Evaluating fibre orientation dispersion in white matter: Comparison of diffusion MRI, histology and polarized light imaging. Neuroimage 157, 561–574. [PubMed: 28602815]

Morozov D, Bar L, Sochen N, Cohen Y, 2013. Modeling of the diffusion MR signal in calibrated model systems and nerves. NMR Biomed. 26, 1787–1795. [PubMed: 24105913]

Nguyen KV, Hernandez-Garzon E, Valette J, 2018. Efficient GPU-based Monte-Carlo simulation of diffusion in real astrocytes reconstructed from confocal microscopy. J. Magn. Reson. 296, 188–199. [PubMed: 30296779]

Nilsson M, Lasic S, Drobnjak I, Topgaard D, Westin CF, 2017. Resolution limit of cylinder diameter estimation by diffusion MRI: The impact of gradient waveform and orientation dispersion. NMR Biomed. 30.

Nilsson M, Latt J, Stahlberg F, van Westen D, Hagslatt H, 2012. The importance of axonal undulation in diffusion MR measurements: a Monte Carlo simulation study. NMR Biomed. 25, 795–805. [PubMed: 22020832]

Novikov DS, Fieremans E, Jespersen SN, Kiselev VG, 2019. Quantifying brain microstructure with diffusion MRI: theory and parameter estimation. NMR Biomed. 32, e3998. [PubMed: 30321478]

Novikov DS, Jensen JH, Helpern JA, Fieremans E, 2014. Revealing mesoscopic structural universality with diffusion. Proc. Natl. Acad. Sci. U. S. A. 111, 5088–5093. [PubMed: 24706873]

Novikov DS, Kiselev VG, Jespersen SN, 2018. On modeling. Magn. Reson. Med. 79, 3172–3193. [PubMed: 29493816]

Nunes D, Cruz TL, Jespersen SN, Shemesh N, 2017. Mapping axonal density and average diameter using non-monotonic time-dependent gradient-echo MRI. J. Magn. Reson. 277, 117–130. [PubMed: 28282586]

Olesen JL, Ostergaard L, Shemesh N, Jespersen SN, 2021. Beyond the diffusion standard model in fixed rat spinal cord with combined linear and planar encoding. Neuroimage 231, 117849. [PubMed: 33582270]

Ong HH, Wehrli FW, 2010. Quantifying axon diameter and intra-cellular volume fraction in excised mouse spinal cord with q-space imaging. Neuroimage 51, 1360–1366. [PubMed: 20350604]

Ong HH, Wright AC, Wehrli SL, Souza A, Schwartz ED, Hwang SN, Wehrli FW, 2008. Indirect measurement of regional axon diameter in excised mouse spinal cord with q-space imaging: simulation and experimental studies. Neuroimage 40, 1619–1632. [PubMed: 18342541]

Ozarslan E, 2009. Compartment shape anisotropy (CSA) revealed by double pulsed field gradient MR. J. Magn. Reson. 199, 56–67. [PubMed: 19398210]

Özarslan E, Koay CG, Shepherd TM, Komlosh ME, İrfanoğlu MO, Pierpaoli C, Basser PJ, 2013. Mean apparent propagator (MAP) MRI: A novel diffusion imaging method for mapping tissue microstructure. Neuroimage 78, 16–32. [PubMed: 23587694]

Özarslan E, Shepherd TM, Koay CG, Blackband SJ, Basser PJ, 2012. Temporal scaling characteristics of diffusion as a new MRI contrast: Findings in rat hippocampus. Neuroimage 60, 1380–1393. [PubMed: 22306798]

Palombo M, Alexander DC, Zhang H, 2019. A generative model of realistic brain cells with application to numerical simulation of the diffusion-weighted MR signal. Neuroimage 188, 391–402. [PubMed: 30553045]

Palombo M, Ianus A, Guerreri M, Nunes D, Alexander DC, Shemesh N, Zhang H, 2020. SANDI: A compartment-based model for non-invasive apparent soma and neurite imaging by diffusion MRI. Neuroimage 215, 116835. [PubMed: 32289460]

Panagiotaki E, Schneider T, Siow B, Hall MG, Lythgoe MF, Alexander DC, 2012. Compartment models of the diffusion MR signal in brain white matter: a taxonomy and comparison. Neuroimage 59, 2241–2254. [PubMed: 22001791]

Pathak S, Schneider W, Zuccolotto A, Huang S, Fan Q, Witzel T, Wald LL, Fieremans E, Komlosh ME, Benjamini D, Avram AV, Basser PJ, 2020. Diffusion ground truth quantification of axon scale phantom: Limits of diffusion MRI on 7T. 3T and Connectome 1.0 International Society for Magnetic Resonance in Medicine.

Peca J, Feliciano C, Ting JT, Wang W, Wells MF, Venkatraman TN, Lascola CD, Fu Z, Feng G, 2011. Shank3 mutant mice display autistic-like behaviours and striatal dysfunction. Nature 472, 437–442. [PubMed: 21423165]

Peca J, Feng G, 2012. Cellular and synaptic network defects in autism. Curr. Opin. Neurobiol. 22, 866–872. [PubMed: 22440525]

Penzes P, Cahill ME, Jones KA, VanLeeuwen JE, Woolfrey KM, 2011. Dendritic spine pathology in neuropsychiatric disorders. Nat. Neurosci. 14, 285–293. [PubMed: 21346746]

Ramos-Llorden G, Maffei C, Tian Q, Bilgic B, Witzel T, Keil B, Yendiki A, Huang SY, 2021. Ex-vivo whole human brain high b-value diffusion MRI at 550 micron with a 3T Connectom scanner. In: Annual Meeting of the International Society of Magnetic Resonance in Medicine, Virtual Meeting, p. 300.

Ramos-Llorden G, Ning L, Liao C, Mukhometzianov R, Michailovich O, Setsompop K, Rathi Y, 2020. High-fidelity, accelerated whole-brain submillimeter in vivo diffusion MRI using gSlider-spherical ridgelets (gSlider-SR). Magn. Reson. Med. 84, 1781–1795. [PubMed: 32125020]

Reischauer C, Staempfli P, Jaermann T, Boesiger P, 2009. Construction of a temperature-controlled diffusion phantom for quality control of diffusion measurements. J. Magn. Reson. Imaging 29, 692–698. [PubMed: 19243053]

Richardson S, Siow B, Batchelor AM, Lythgoe MF, Alexander DC, 2013. A viable isolated tissue system: a tool for detailed MR measurements and controlled perturbation in physiologically stable tissue. Magn. Reson. Med. 69, 1603–1610. [PubMed: 22821404]

Roebroeck A, Miller KL, Aggarwal M, 2019. Ex vivo diffusion MRI of the human brain: Technical challenges and recent advances. NMR Biomed. 32, e3941. [PubMed: 29863793]

Safadi Z, Grisot G, Jbabdi S, Behrens TE, Heilbronner SR, McLaughlin NCR, Mandeville J, Versace A, Phillips ML, Lehman JF, Yendiki A, Haber SN, 2018. Functional segmentation of the anterior

limb of the internal capsule: linking white matter abnormalities to specific connections. J. Neurosci. 38, 2106–2117. [PubMed: 29358360]

Schmitt F, Stehling MK, Turner R, 2012. Echo-Planar Imaging: Theory, Technique and Application. Springer Science & Business Media.

Scholz A, Etzel R, May MW, Mahmutovic M, Tian Q, Ramos-Llorden G, Maffei C, Bilgic B, Witzel T, Stockmann JP, Mekkaoui C, Wald LL, Huang SY, Yendiki A, Keil B, 2021. A 48-channel receive array coil for mesoscopic diffusion-weighted MRI of ex vivo human brain on the 3 T connectome scanner. Neuroimage 238, 118256. [PubMed: 34118399]

Scholz A, May M, Etzel R, Mahmutovic M, Kutscha N, Wald LL, Yendiki A, Keil B, 2019. A 48-channel ex vivo brain array coil for diffusion-weighted MRI at 3T. In: Proceedings of the 27th Annual Meeting of the ISMRM, Montreal, Canada, p. 1494.

Setsompop K, Fan Q, Stockmann J, Bilgic B, Huang S, Cauley SF, Nummenmaa A, Wang F, Rathi Y, Witzel T, Wald LL, 2017. High-resolution in vivo diffusion imaging of the human brain with generalized slice dithered enhanced resolution: simultaneous multislice (gSlider-SMS). Magn. Reson. Med..

Setsompop K, Gagoski BA, Polimeni JR, Witzel T, Wedeen VJ, Wald LL, 2012. Blipped-controlled aliasing in parallel imaging for simultaneous multislice echo planar imaging with reduced g-factor penalty. Magn. Reson. Med. 67, 1210–1224. [PubMed: 21858868]

Setsompop K, Kimmlingen R, Eberlein E, Witzel T, Cohen-Adad J, McNab JA, Keil B, Tisdall MD, Hoecht P, Dietz P, Cauley SF, Tountcheva V, Matschl V, Lenz VH, Heberlein K, Potthast A, Thein H, Van Horn J, Toga A, Schmitt F, Lehne D, Rosen BR, Wedeen V, Wald LL, 2013. Pushing the limits of in vivo diffusion MRI for the Human Connectome Project. Neuroimage 80, 220–233. [PubMed: 23707579]

Shemesh N, Cohen Y, 2011. Microscopic and compartment shape anisotropies in gray and white matter revealed by angular bipolar double-PFG MR. Magn. Reson. Med. 65, 1216–1227. [PubMed: 21305595]

Shemesh N, Ozarslan E, Adiri T, Basser PJ, Cohen Y, 2010a. Noninvasive bipolar double-pulsed-field-gradient NMR reveals signatures for pore size and shape in polydisperse, randomly oriented, inhomogeneous porous media. J. Chem. Phys. 133, 044705. [PubMed: 20687674]

Shemesh N, Ozarslan E, Komlosh ME, Basser PJ, Cohen Y, 2010b. From single-pulsed field gradient to double-pulsed field gradient MR: gleaning new microstructural information and developing new forms of contrast in MRI. NMR Biomed. 23, 757–780. [PubMed: 20690130]

Stanisz GJ, Szafer A, Wright GA, Henkelman RM, 1997. An analytical model of restricted diffusion in bovine optic nerve. Magn. Reson. Med. 37, 103–111. [PubMed: 8978638]

Swanson LW, Lichtman JW, 2016. From cajal to connectome and beyond. Annu. Rev. Neurosci. 39, 197–216. [PubMed: 27442070]

Szczepankiewicz F, Lasic S, van Westen D, Sundgren PC, Englund E, Westin CF, Stahlberg F, Latt J, Topgaard D, Nilsson M, 2015. Quantification of microscopic diffusion anisotropy disentangles effects of orientation dispersion from microstructure: applications in healthy volunteers and in brain tumors. Neuroimage 104, 241–252. [PubMed: 25284306]

Szczepankiewicz F, Westin CF, Nilsson M, 2021. Gradient waveform design for tensor-valued encoding in diffusion MRI. J. Neurosci. Methods 348, 109007. [PubMed: 33242529]

Tan ET, Hua Y, Fiveland EW, Vermilyea ME, Piel JE, Park KJ, Ho VB, Foo TKF, 2019. Peripheral nerve stimulation limits of a high amplitude and slew rate magnetic field gradient coil for neuroimaging. Magn. Reson. Med..

Tapia JC, Kasthuri N, Hayworth KJ, Schalek R, Lichtman JW, Smith SJ, Buchanan J, 2012. High-contrast en bloc staining of neuronal tissue for field emission scanning electron microscopy. Nat. Protoc. 7, 193–206. [PubMed: 22240582]

Tax CMW, Szczepankiewicz F, Nilsson M, Jones DK, 2020. The dot-compartment revealed? Diffusion MRI with ultra-strong gradients and spherical tensor encoding in the living human brain. Neuroimage 210, 116534. [PubMed: 31931157]

Teh I, McClymont D, Burton RA, Maguire ML, Whittington HJ, Lygate CA, Kohl P, Schneider JE, 2016. Resolving fine cardiac structures in rats with high--resolution diffusion tensor imaging. Sci. Rep. 6, 30573. [PubMed: 27466029]

Tian Q, Ngamsombat C, Lee HH, Berger DR, Wu Y, Fan Q, Bilgic B, Novikov DS, Fieremans E, Rosen BR, Lichtman JW, Huang SY, 2020. Automated segmentation of human axon and myelin from electron microscopy data using deep learning for microstructural validation and simulation. Proc. Intl. Soc. Mag. Reson. Med. 28.

Topgaard D, 2017. Multidimensional diffusion MRI. J. Magn. Reson. 275, 98–113. [PubMed: 28040623]

Ugurbil K, Xu J, Auerbach EJ, Moeller S, Vu AT, Duarte-Carvajalino JM, Lenglet C, Wu X, Schmitter S, Van de Moortele PF, Strupp J, Sapiro G, De Martino F, Wang D, Harel N, Garwood M, Chen L, Feinberg DA, Smith SM, Miller KL, Sotiropoulos SN, Jbabdi S, Andersson JL, Behrens TE, Glasser MF, Van Essen DC, Yacoub E, Consortium, W.U.-M.H., 2013. Pushing spatial and temporal resolution for functional and diffusion MRI in the Human Connectome Project. Neuroimage 80, 80–104. [PubMed: 23702417]

Van Vaals J, Bergman A, 1990. Optimization of eddy-current compensation. J. Magn. Reson. 90, 52–70 (1969).

Veraart J, Fieremans E, Novikov DS, 2019. On the scaling behavior of water diffusion in human brain white matter. Neuroimage 185, 379–387. [PubMed: 30292815]

Veraart J, Nunes D, Rudrapatna U, Fieremans E, Jones DK, Novikov DS, Shemesh N, 2020. Nonivasive quantification of axon radii using diffusion MRI. Elife 9.

Wang F, Dong Z, Tian Q, Liao C, Fan Q, Hoge WS, Keil B, Polimeni JR, Wald LL, Huang SY, Setsompop K, 2020. In vivo human whole-brain Connectom diffusion MRI dataset at 760 μm isotropic resolution. bioRxiv.

Wang F, Dong Z, Tian Q, Liao C, Fan Q, Hoge WS, Keil B, Polimeni JR, Wald LL, Huang SY, Setsompop K, 2021. In vivo human whole-brain Connectom diffusion MRI dataset at 760 microm isotropic resolution. Sci. Data 8, 122. [PubMed: 33927203]

Waxman SG, Kocsis JD, Stys PK, 1995. The Axon: Structure, Function and Pathophysiology. Oxford University Press, New York.

Weiger M, Overweg J, Rösler MB, Froidevaux R, Hennel F, Wilm BJ, Penn A, Sturzenegger U, Schuth W, Mathlener M, Borgo M, Börnert P, Leussler C, Luechinger R, Dietrich BE, Reber J, Brunner DO, Schmid T, Vionnet L, Pruessmann KP, 2017. A high-performance gradient insert for rapid and short-T2 imaging at full duty cycle. Magn. Reson. Med..

Westin CF, Knutsson H, Pasternak O, Szczepankiewicz F, Ozarslan E, van Westen D, Mattisson C, Bogren M, O'Donnell LJ, Kubicki M, Topgaard D, Nilsson M, 2016. Q-space trajectory imaging for multidimensional diffusion MRI of the human brain. Neuroimage 135, 345–362. [PubMed: 26923372]

Wieseotte C, Witzel T, Polimeni J, Nummenmaa A, Gruber B, Schreiber LM, Wald LL, 2015. Pushing the limits of ex-vivo diffusion MRI and tractography of the human brain. In: Proceedings of the 23rd Annual Meeting of the ISMRM, Toronto, Canada, p. 2847.

Wilm BJ, Barmet C, Pavan M, Pruessmann KP, 2011. Higher order reconstruction for MRI in the presence of spatiotemporal field perturbations. Magn. Reson. Med. 65, 1690–1701. [PubMed: 21520269]

Wilm BJ, Nagy Z, Barmet C, Vannesjo SJ, Kasper L, Haeberlin M, Gross S, Dietrich BE, Brunner DO, Schmid T, 2015. Diffusion MRI with concurrent magnetic field monitoring. Magn. Reson. Med. 74, 925–933. [PubMed: 26183218]

Winkler SA, Schmitt F, Landes H, de Bever J, Wade T, Alejski A, Rutt BK, 2018. Gradient and shim technologies for ultra high field MRI. Neuroimage 168, 59–70. [PubMed: 27915120]

Xu J, 2021. Probing neural tissues at small scales: Recent progress of oscillating gradient spin echo (OGSE) neuroimaging in humans. J. Neurosci. Methods 349, 109024. [PubMed: 33333089]

Xu J, Li H, Harkins KD, Jiang X, Xie J, Kang H, Does MD, Gore JC, 2014. Mapping mean axon diameter and axonal volume fraction by MRI using temporal diffusion spectroscopy. Neuroimage 103, 10–19. [PubMed: 25225002]

Xu T, Foxley S, Kleinnijenhuis M, Chen WC, Miller KL, 2018. The effect of realistic geometries on the susceptibility-weighted MR signal in white matter. Magn. Reson. Med. 79, 489–500. [PubMed: 28394030]

Yang G, Tian Q, Leuze C, Wintermark M, McNab JA, 2018. Double diffusion encoding MRI for the clinic. Magn. Reson. Med. 80, 507–520. [PubMed: 29266375]

Yendiki A,..., 2021. Postmortem validation of the connectome. Neuroimage.

Zhang B, Yen YF, Chronik BA, McKinnon GC, Schaefer DJ, Rutt BK, 2003. Peripheral nerve stimulation properties of head and body gradient coils of various sizes. Magn. Reson. Med. 50, 50–58. [PubMed: 12815678]

Zhang H, Hubbard PL, Parker GJ, Alexander DC, 2011. Axon diameter mapping in the presence of orientation dispersion with diffusion MRI. Neuroimage 56, 1301–1315. [PubMed: 21316474]

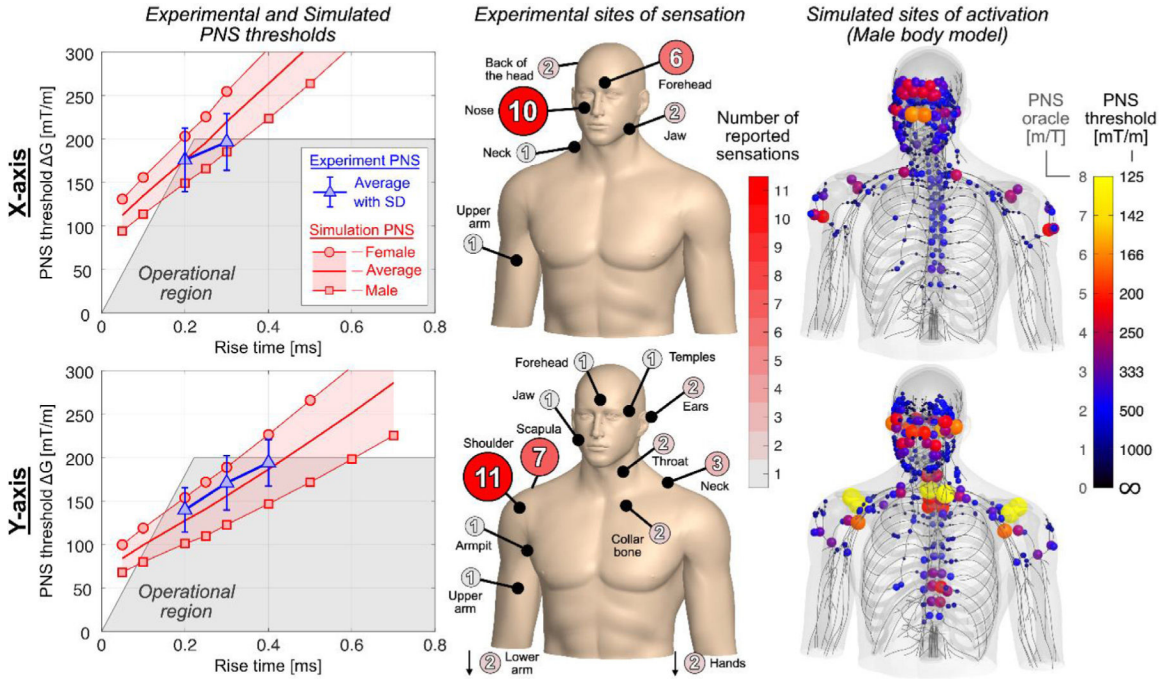

Fig. 1.

Peripheral nerve stimulation (PNS) characteristics of the Siemens Impulse head gradient obtained in experiments and simulations using realistic body models. Left column: Experimental PNS thresholds (blue) and simulated thresholds (red, for the female and male model and their average) in terms of the smallest stimulating gradient amplitude as a function of trapezoidal rise time for the Siemens Impulse head gradient (G_{max} = 200 mT/m, maximum slew rate of 900 T/m/s), the geometry of which is being adopted for the Connectome 2.0 head gradient with modified windings to achieve the target G_{max} = 500 mT/m and maximum slew rate of 600 T/m/s. The gray shaded area denotes the accessible performance region determined by G_{max} and maximum slew rate. Center column: Sites of perceived sensation reported by the subjects during the stimulation experiments. Right column: Predicted sites of activation in the male body model. The color and size of each sphere correspond to the reciprocal PNS threshold (which we refer to as the PNS oracle). Figure adapted from Davids et al. (2021a).

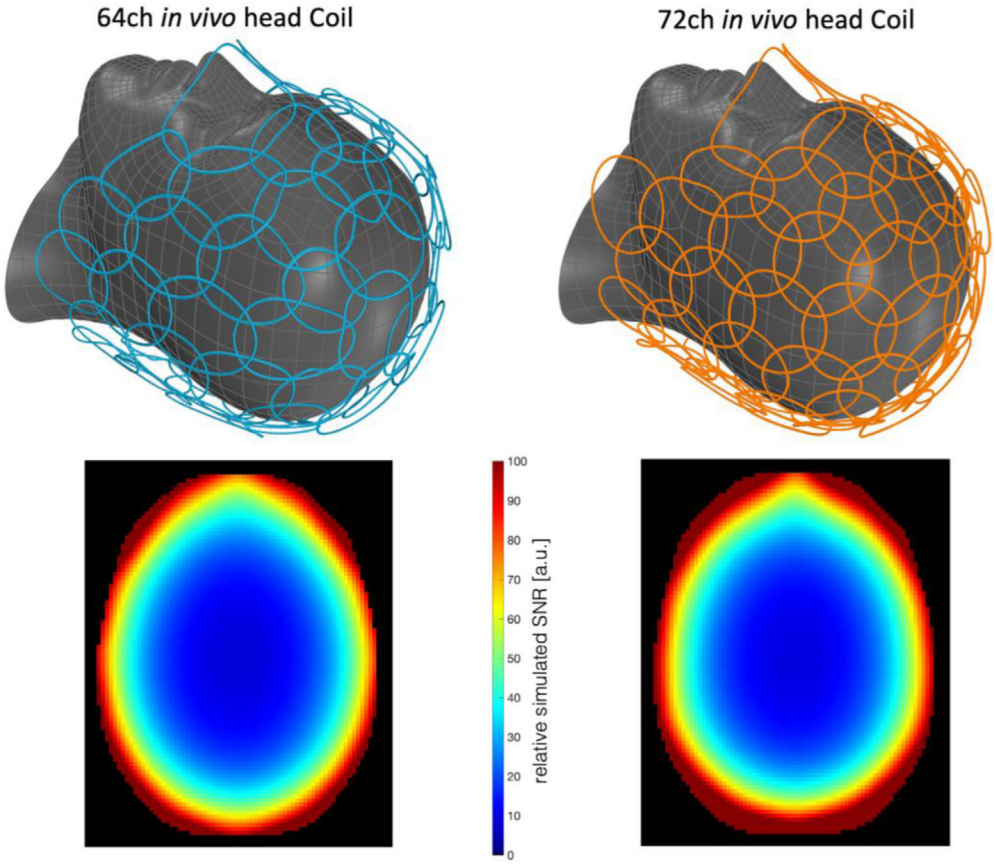

Fig. 2.

64-channel and 72-channel *in vivo* head array coil configurations (top row) with simulated SNR maps (bottom row). Both head coil designs show similar SNR performance at the center of the phantom. In the periphery of the brain, the 72-channel head coil shows a 13% improvement in the simulated SNR. The latter will be advantageous for studies of cortical microstructure.

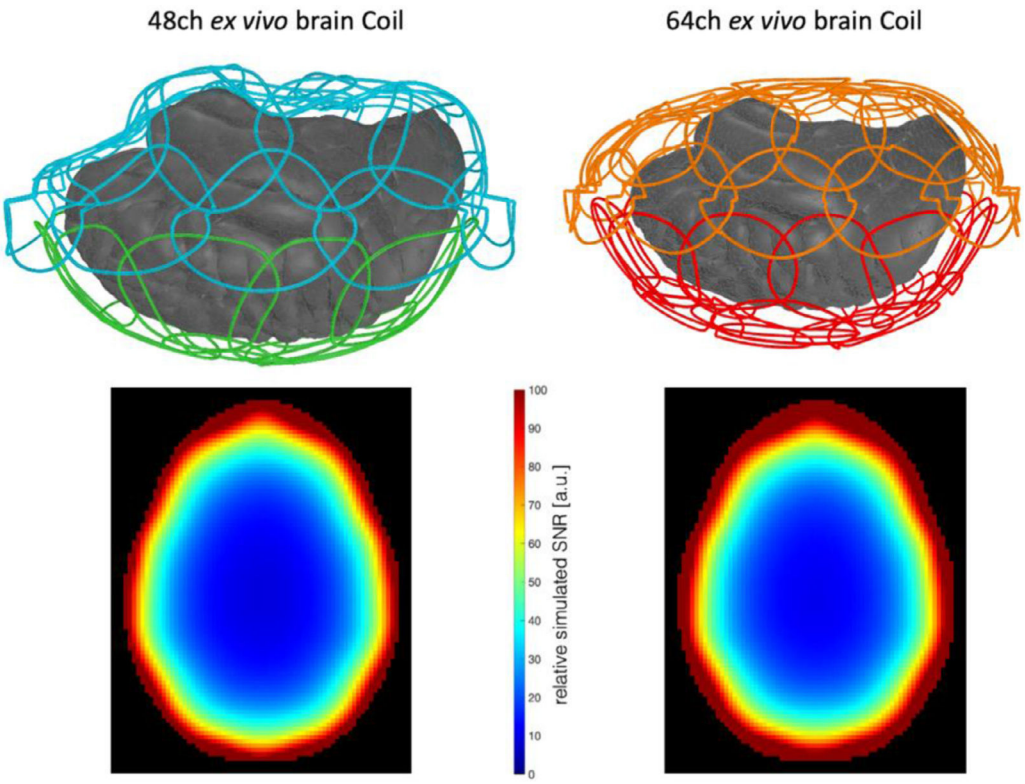

Fig. 3.

48-channel and 64-channel *ex vivo* whole brain array coil configurations (top row) with simulated SNR maps (bottom row). The dedicated 64-channel *ex vivo* brain array enables approximately 17% higher SNR in the corresponding cortical regions of the phantom, while achieving nearly identical SNR in the central region.

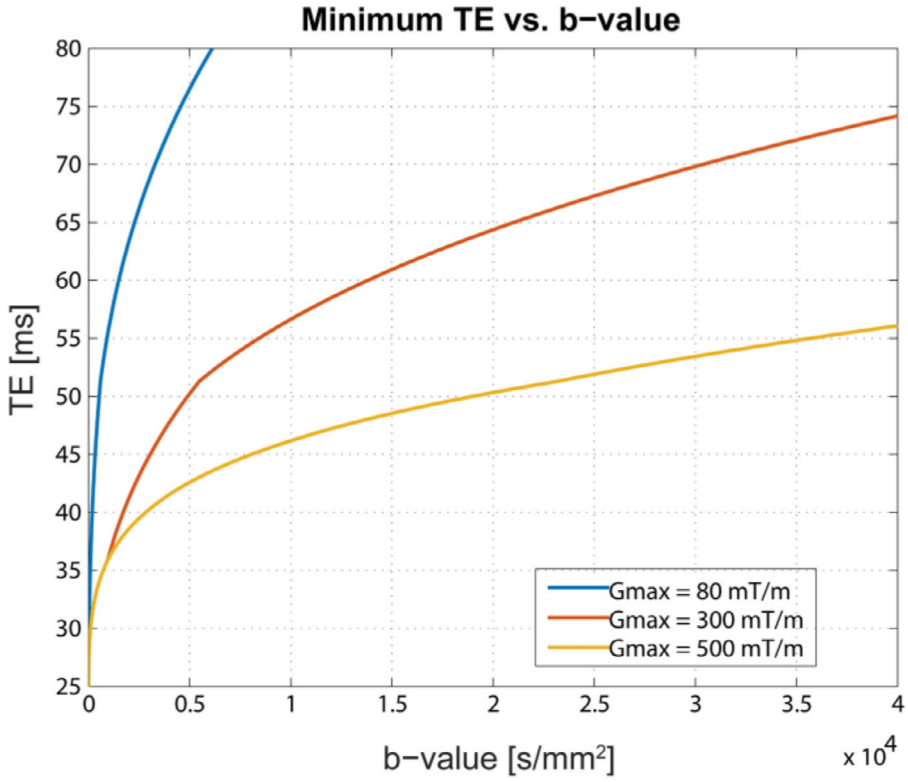

Fig. 4.

Minimum TE obtained for the pulsed gradient spin echo diffusion sequence as a function of b-value for different maximum gradient strengths.

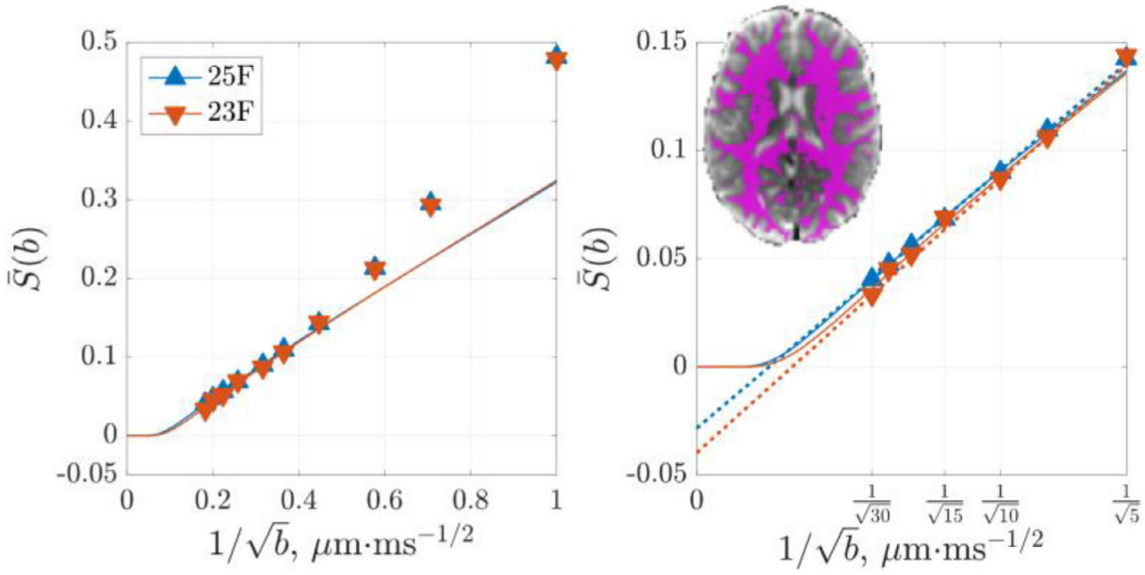

Fig. 5.

In brain white matter of two human subjects, the directionally averaged diffusion signal $\bar{S}(b)$ scales as ~$1/\sqrt{b}$ at strong diffusion weighting b. At high b-value, the extra-axonal signal decays exponentially fast, and the "stick"-like intra-axonal signal dominates. The deviation of the signal power-law scaling (solid line), manifested by the negative intercept in $b \to \infty$ limit (dotted line), offers an estimate for the effective axonal radius $r_{\text{eff}} \approx 3$ μm.

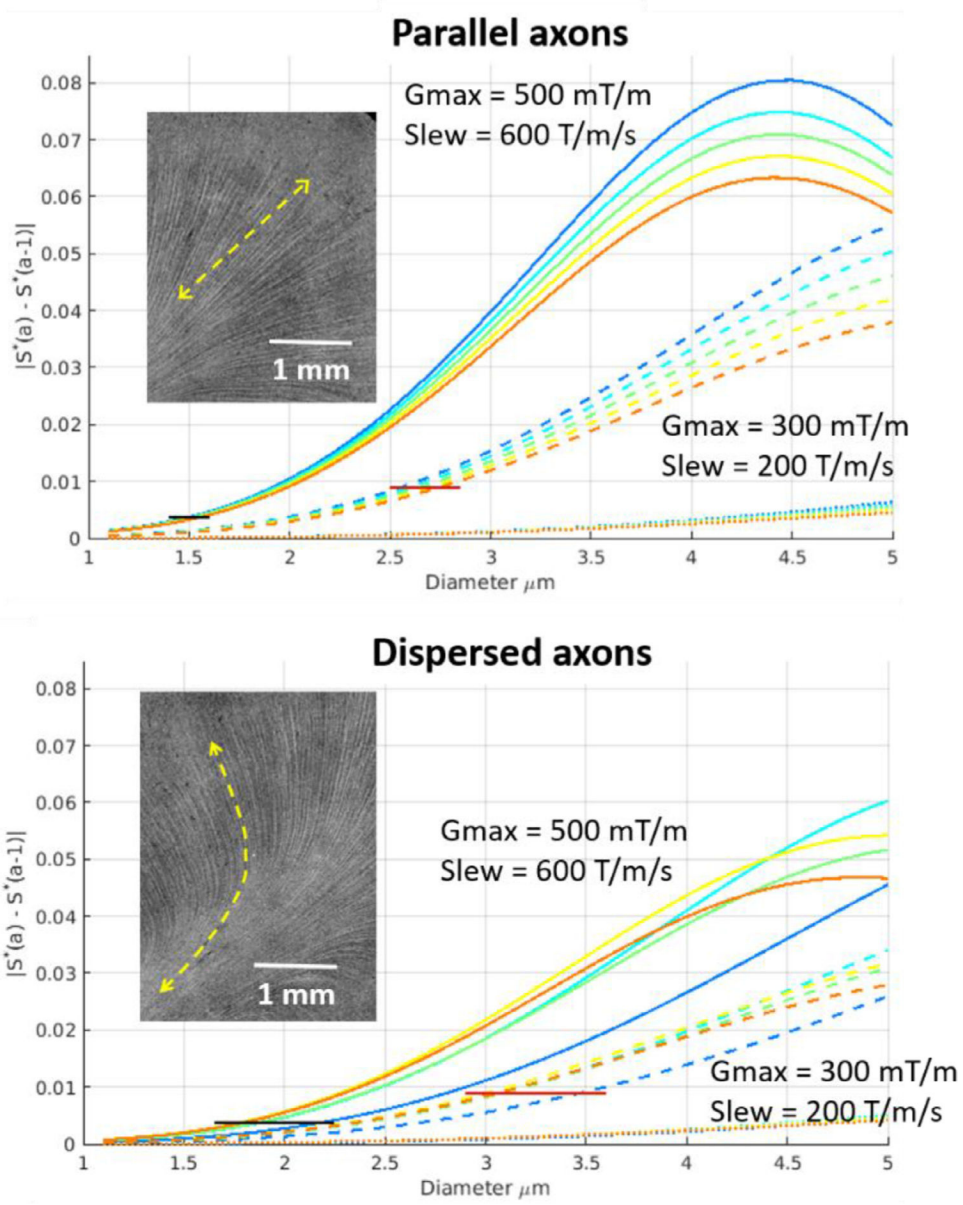

Fig. 6.

Simulation results showing the resolution limit of PGSE (blue) and OGSE (other colors) for the next-generation ultra-high G_{max}/slew rate of 500 mT/m / 600T/m/s (solid lines) versus the current G_{max}/slew rate of 300mT/m / 200 T/m/s (dashed lines). Simulation results for (TOP) parallel cylinders and (BOTTOM) dispersed cylinders mimicking axons (inset: OCT images of axons in the human temporal lobe). The shorter effective TE achievable with the next-generation Connectome scanner will enable a nearly 2x increase in SNR, which sets the resolution limit (horizontal bars), resulting in a minimum axonal size of 1.4–1.6 μm vs. 2.5–3 μm (Connectome 2.0 vs 1.0) in the case of parallel axons, and 1.6 μm vs. 3 μm in the case of dispersed axons for relatively low-frequency OGSE. The different OGSE curves (denoted by cyan, green, yellow and orange) correspond to different OGSE frequencies. The dotted lines at the bottom of each figure correspond to a G_{max} and slew rate of 80 mT/m and 200

T/m/s, respectively, representing the resolution limit attainable with the latest commercially available clinical gradient systems. Simulations were performed using the Microstructure Imaging Sequence Simulation ToolBox (MISST) (Drobnjak et al., 2010; Drobnjak et al., 2011; Ianus et al., 2013).

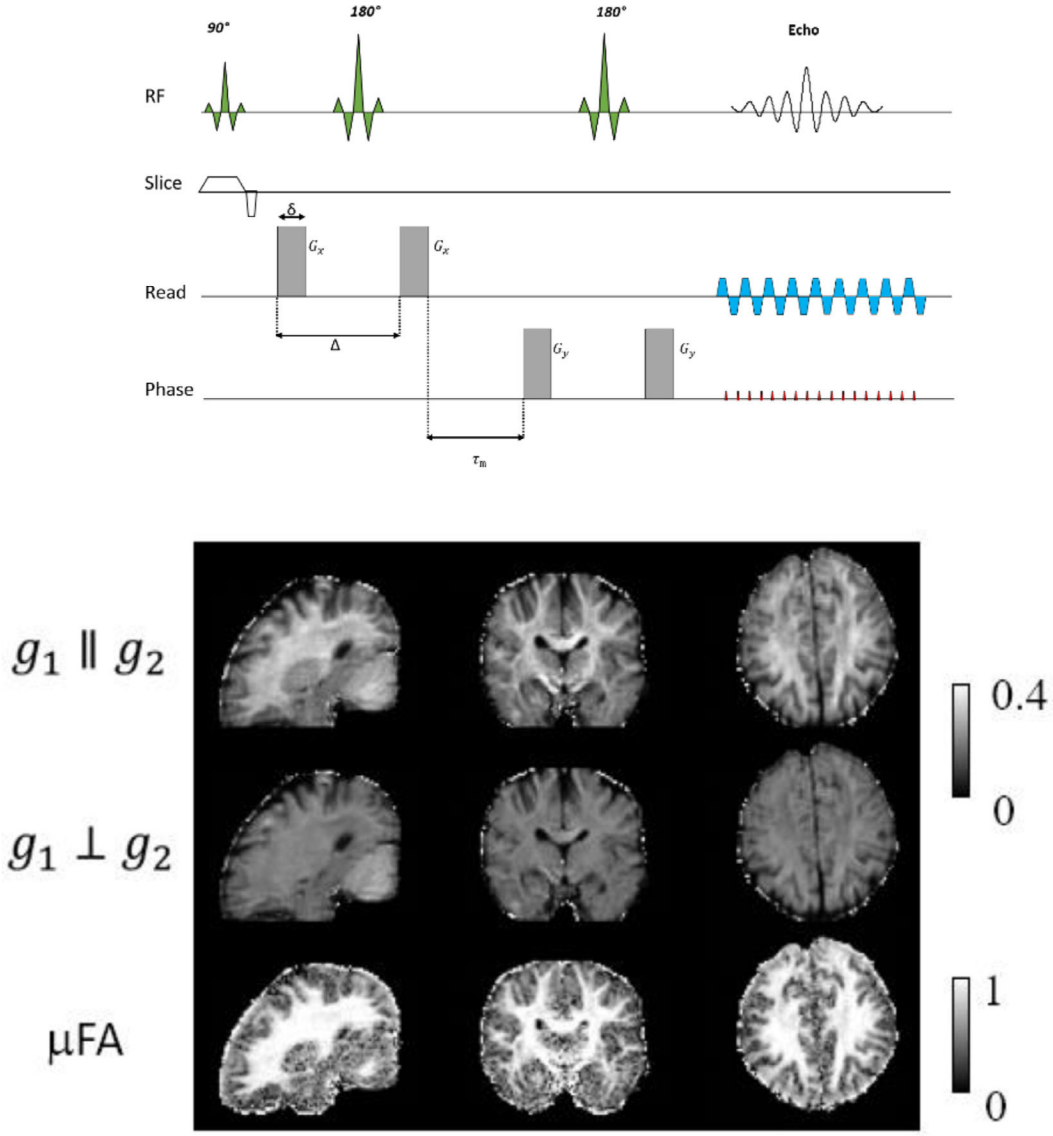

Fig. 7.

Double diffusion-encoding (DDE) sequence (top) and maps of mean diffusion-weighted imaging volumes using parallel and perpendicular diffusion encoding directions (bottom). The microscopy anisotropy (μFA) maps derived from the difference of the parallel and perpendicular signals is shown on the bottom panel. Figure adapted from Fan et al. (2020b).

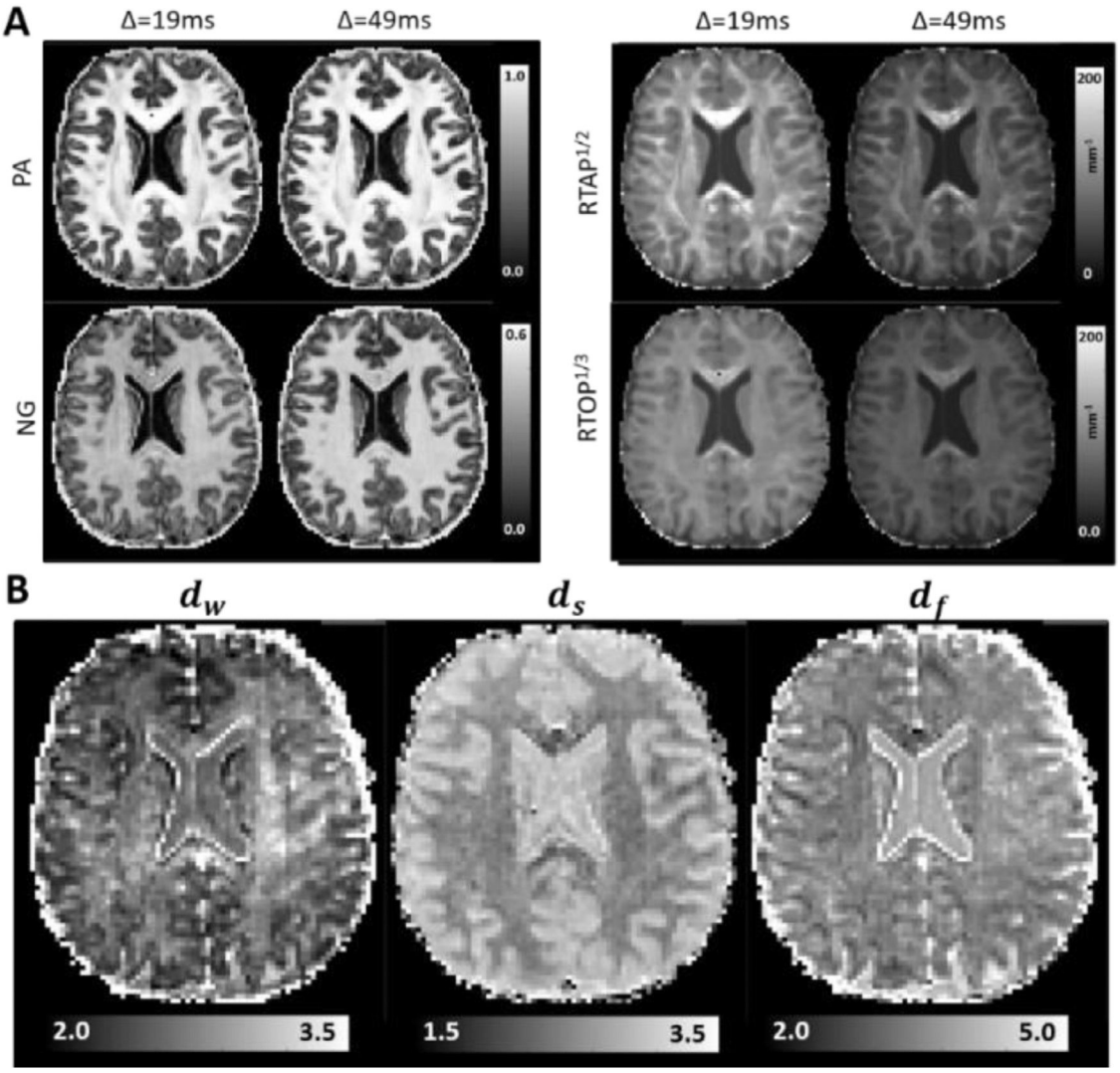

Fig. 8.

A. The diffusion time (Δ) dependence of MAP-MRI scalar parameters (Avram et al., 2016; Özarslan et al., 2013) in a healthy volunteer (Avram et al., 2021): Propagator Anisotropy (PA); Non-Gaussianity (NG); Return-to-axis probability (RTAP); and Return-to-origin-probability (RTOP). B. The corresponding temporal scaling MRI parameters (Özarslan et al., 2012) by representing brain tissue as fractal-like media: d_w – statistical fractal dimension; d_s – spectral dimension; d_f – fractal dimension. Figure adapted from Avram et al. (2021).

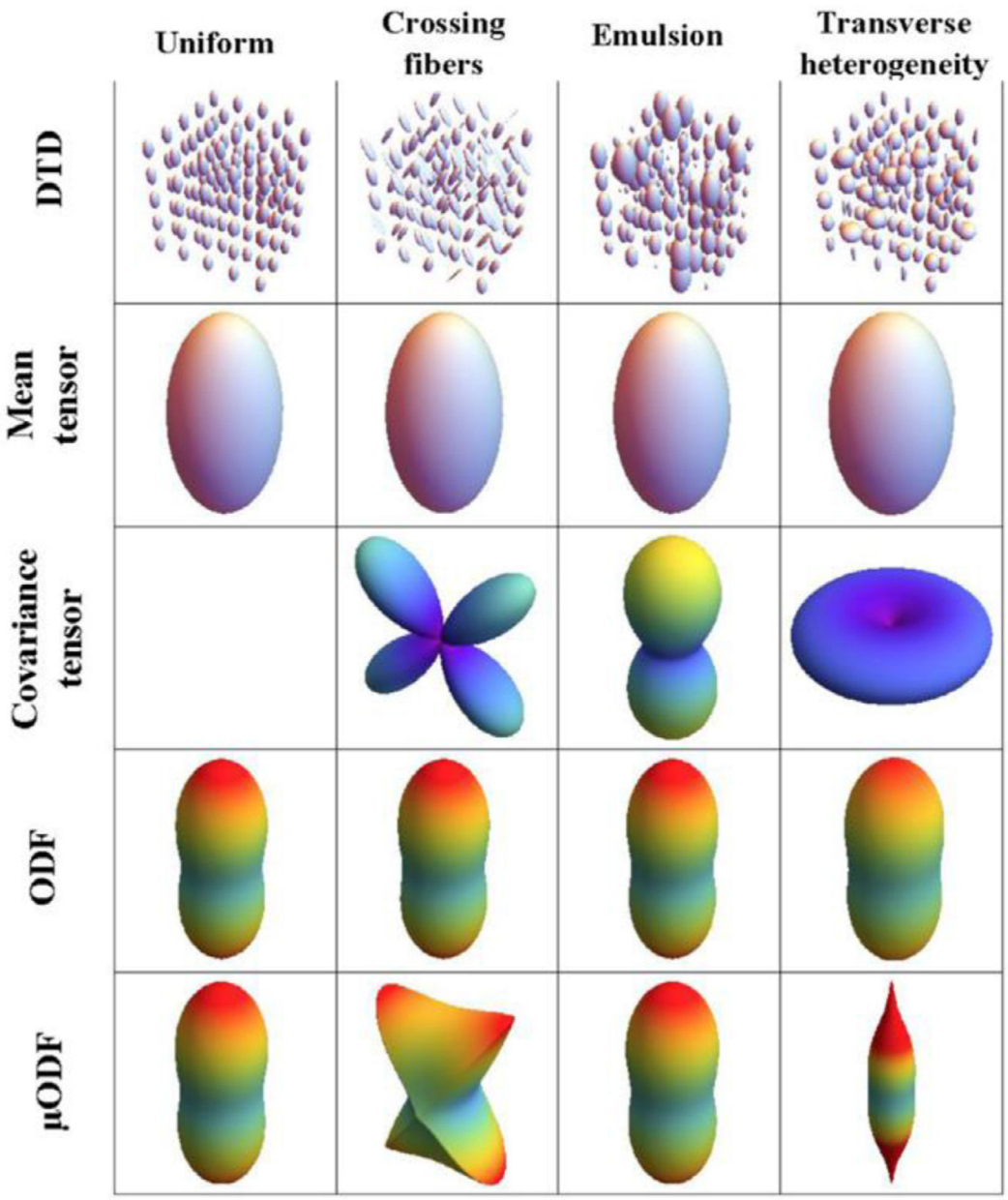

Fig. 9.

Different microstructural "motifs" derived from the covariance of the subvoxel diffusion tensor distribution (Magdoom et al., 2021). ODF – Orientation distribution function, μODF – micro-ODF. Figure adapted from Magdoom et al. (2021).

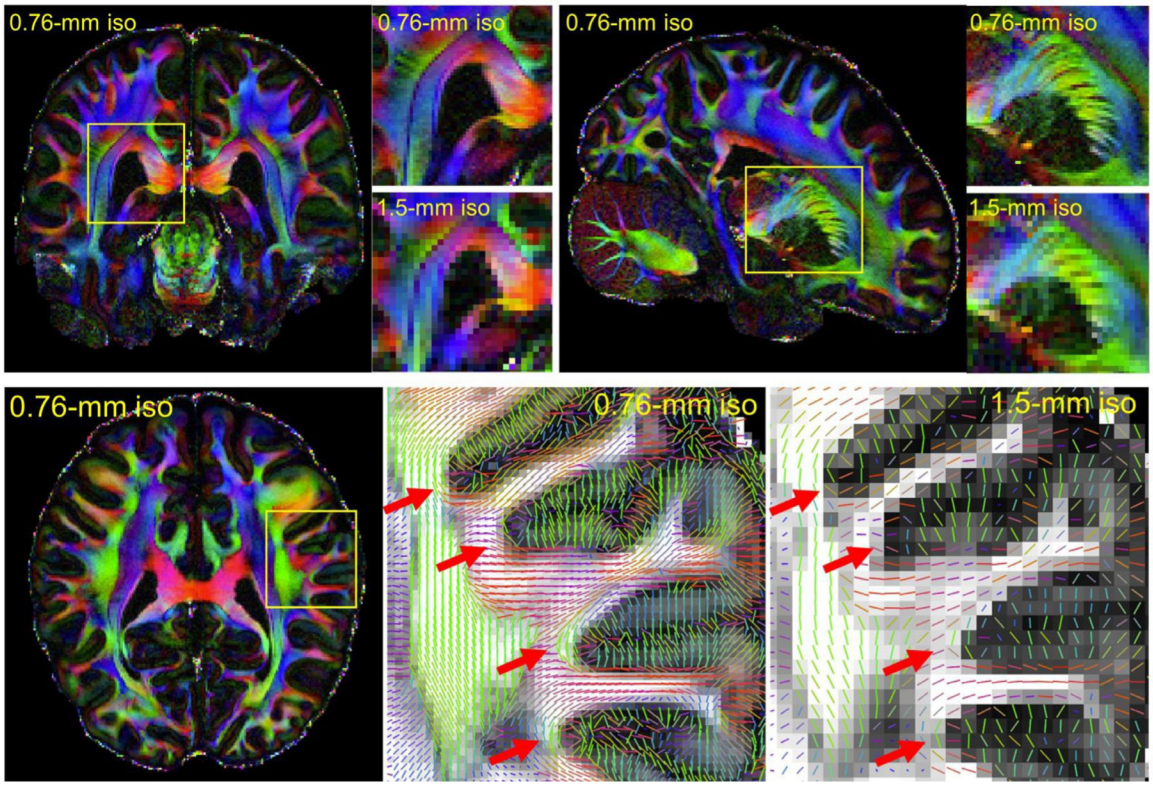

Fig. 10.

High-quality dMRI reference dataset acquired at 760 μm isotropic resolution with 1260 q-space samplings across 9 two-hour sessions on a single healthy participant. The creation of this benchmark dataset was made possible through the use of the current Connectome scanner, a custom-built 64-channel phased-array head coil, and a recently developed SNR-efficient gSlider acquisition. The color-coded FA maps of the 0.76-mm dataset are presented in three orthogonal views. By using high spatial resolution, improved visualization of detailed structures is provided (top panel), and more sharping-turning fibers such as those connecting cortical regions between adjacent gyri can be observed (red arrows, bottom panel). Figure adapted from Wang et al. (2021).

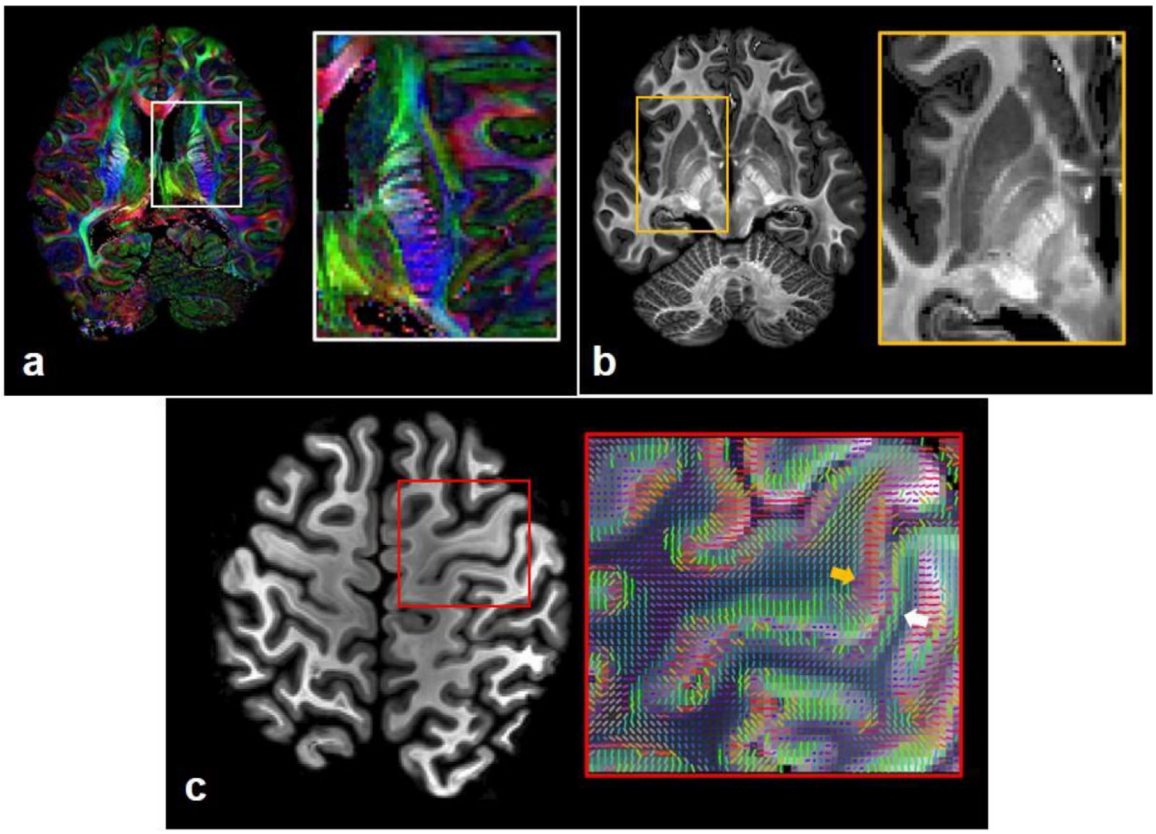

Fig. 11.

Axial post-mortem whole human brain images obtained with multi-shell diffusion MRI at 0.73 mm isotropic resolution using b-values of 4,000 s/mm^2 and 10,000 s/mm^2. (a) Colorized FA maps obtained from DTI analysis of the b = 4,000 s/mm^2 data depict the fine gray-matter bridges spanning the internal capsule. (b) Mean kurtosis maps obtained from diffusion kurtosis analysis of the b-values of 4,000 s/mm^2 and 10,000 s/mm^2 delineate the external capsule, putamen, and subcortical nuclei with exquisite detail. There is also high mean kurtosis corresponding to the corticospinal tracts coursing through the cerebral peduncles. (c) Mean diffusion-weighted image at b = 10,000 s/mm^2 (left) and primary eigenvectors derived from DTI analysis of the b = 4,000 s/mm^2 data show primarily radial fibers (orange arrow) in the hand knob of the precentral gyrus (primary motor cortex) and a thin layer of tangential fibers (white arrow) in the postcentral gyrus (primary somatosensory cortex) on the opposite side of the central sulcus. Figure panels (a) and (b) adapted from Scholz et al. (2021).

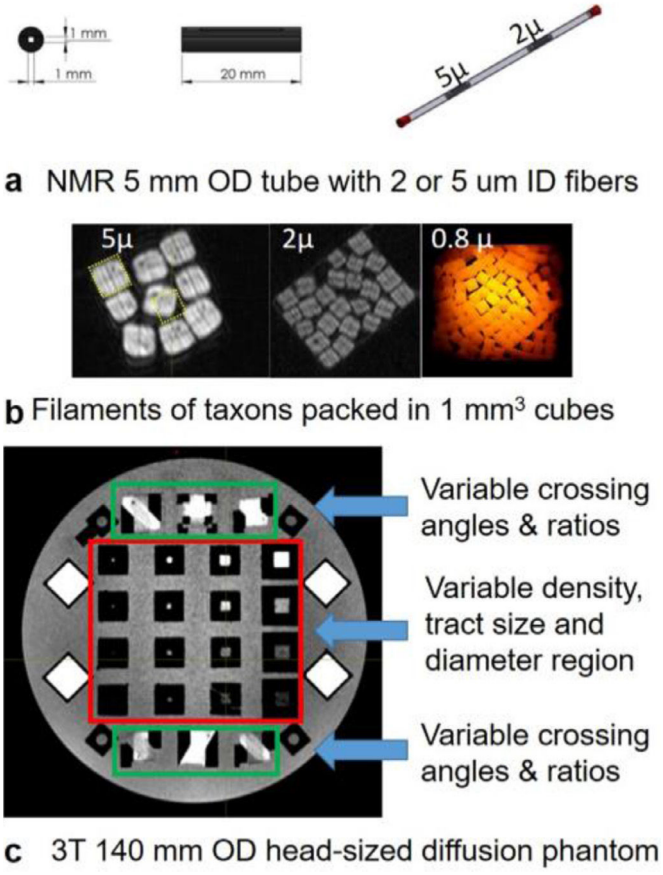

Fig. 12.

Multi-scale taxon phantoms designed for imaging on preclinical and human MRI systems. (a) Micro-phantom manufactured to fit in a 5-mm NMR tube containing fibers of 5 μm and 2 μm inner diameter (ID). (b) Filaments packed into a 1 mm^3 cube for fibers of three diameters (5 μm, 2 μm and 0.8 μm). Each filament contains 3476 taxon tubes. (c) 3T phantom with crossing fibers (green areas) and variable packing density cubes of different size (1, 2, 4, and 6 mm on a side) and density (0.125, 0.25, 0.50, and 1.0). The phantom was sized to fit in a standard 20-cm head coil. Figure adapted from Pathak et al. (2020).

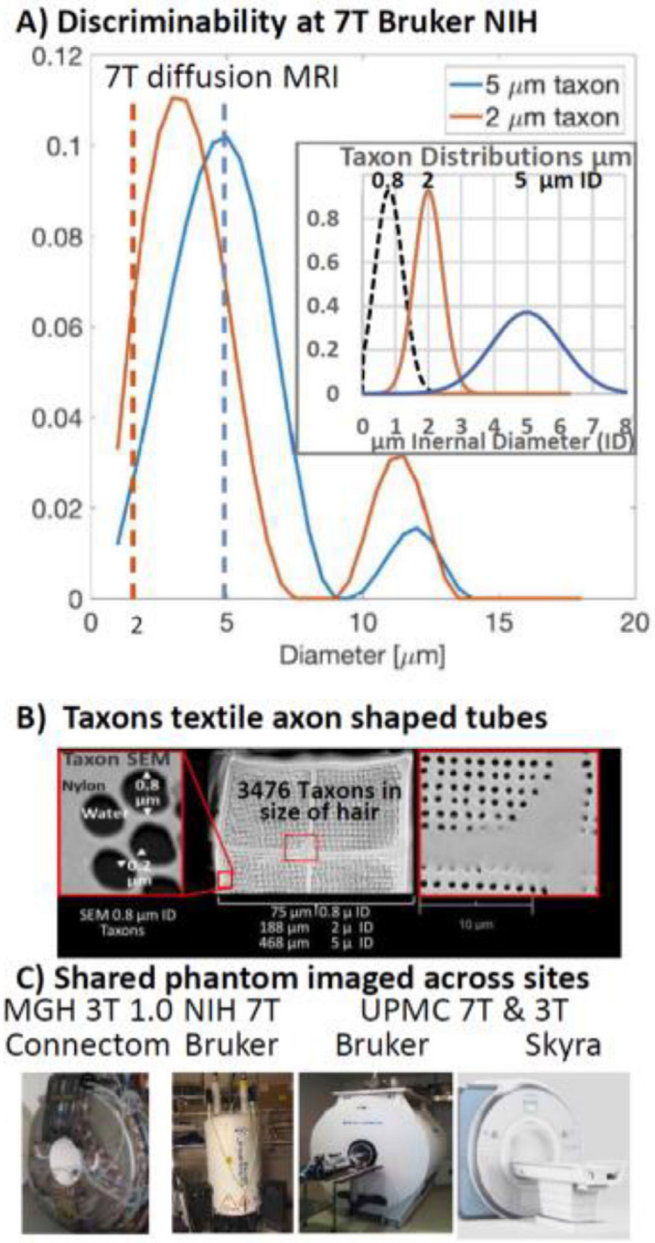

Fig. 13.

Ground-truth diffusion phantom shared across labs demonstrate discrimination of fibers of 2 and 5 um in diameter. (a) NMR tube phantom containing 2 and 5 μm ID taxons. The 2 and 5 μm peaks are distinguishable based on a DDE acquisition with analysis using the non-parametric multiple correlation functions framework. **(b)** Scanning electron microscope image of the taxons. **(c)** Phantom was scanned on: the Connectome scanner at MGH, Bruker 7T at NIH, and Skyra 3T and 7T Bruker systems at UPMC. Figure adapted from Pathak et al. (2020).

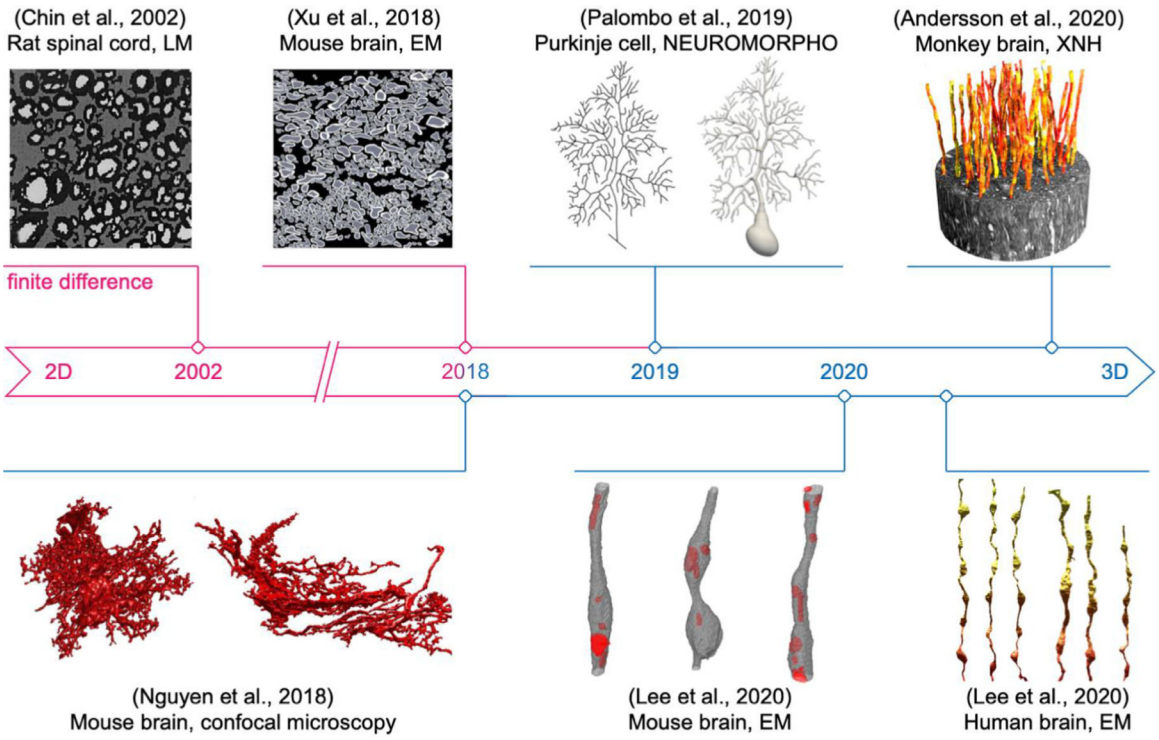

Fig. 14.

The progression of diffusion simulations in realistic tissue microstructure. Starting from diffusion simulations in 2-dimensional rodent light microscopy (LM) and electron microscopy (EM) data, the advance of microscopy techniques and cell segmentation pipeline have pushed forward the research of diffusion simulations in 3-dimensional tissue micro-geometry, such as sequential slice EM and synchrotron X-ray nano-holotomography (XNH) in primate brain white matter. The figure is adapted from Andersson et al. (2020), Chin et al. (2002), Lee et al. (2020c), Lee et al. (2020e), Nguyen et al. (2018), Palombo et al. (2019) and Xu et al. (2018) with permission from Wiley, Elsevier, and Springer Nature.